

1 **REGULATION OF MELANOCYTE DEVELOPMENT BY LIGAND-DEPENDENT BMP**
2 **SIGNALING UNDERLIES ONCOGENIC BMP SIGNALING IN MELANOMA**

3
4 Alec K. Gramann¹, Arvind M. Venkatesan¹⁺, Melissa Guerin¹, Craig J. Ceol^{1*}

5 1. Program in Molecular Medicine and Department of Molecular, Cell, and Cancer
6 Biology, University of Massachusetts Medical School, 368 Plantation St,
7 Worcester, MA 01605, USA

8 + Present address: Syngene International Ltd., Biocon Park, SEZ, Bommasandra
9 Jigani Link Road, Phase-IV, Bommasandra Industrial Area, Bangalore,
10 Karnataka 560099, India

11
12 *Correspondence: craig.ceol@umassmed.edu

13
14 **Abstract**

15 Preventing terminal differentiation is important in the development and progression of
16 many cancers including melanoma. Recent identification of the BMP ligand *GDF6* as a
17 novel melanoma oncogene showed *GDF6*-activated BMP signaling suppresses
18 differentiation of melanoma cells. Previous studies have identified roles for *GDF6*
19 orthologs during early embryonic and neural crest development, but have not identified
20 direct regulation of melanocyte development by *GDF6*. Here, we investigate the BMP
21 ligand *gdf6a*, a zebrafish ortholog of human *GDF6*, during the development of
22 melanocytes from the neural crest. We establish that the loss of *gdf6a* or inhibition of
23 BMP signaling during neural crest development disrupts normal pigment cell
24 development, leading to an increase in the number of melanocytes and a corresponding
25 decrease in iridophores, another neural crest-derived pigment cell type in zebrafish.
26 This shift occurs as pigment cells arise from the neural crest and depends on *mitfa*, an
27 ortholog of *MITF*, a key regulator of melanocyte development that is also targeted by
28 oncogenic BMP signaling. Together, these results indicate that the oncogenic role

29 ligand-dependent BMP signaling plays in suppressing differentiation in melanoma is a
30 reiteration of its physiological roles during melanocyte development.

31

32 **Keywords**

33 Melanoma, melanocyte, BMP signaling, neural crest, specification, mitf, mitfa, zebrafish

34

35 **Introduction**

36 Tumor differentiation status is often an important prognostic factor in cancer. For many
37 cancer types, tumors that are less differentiated are associated with a higher grade and
38 worse prognosis compared to more differentiated tumors, which often follow indolent
39 courses (Hoek et al., 2006; Rosai & Ackerman, 1979). In order to adopt a less
40 differentiated state, a common event in cancer is downregulation of factors that drive
41 differentiation of adult tissues (Chaffer et al., 2011; Dravis et al., 2018). This loss of pro-
42 differentiation factors is often coupled with an upregulation of other factors that are
43 associated with embryonic or progenitor states (Caramel et al., 2013; Tulchinsky,
44 Pringle, Caramel, & Ansieau, 2014). Thus, many de-differentiated and high-grade
45 cancers have gene expression profiles associated with early development (O'Brien-Ball
46 & Biddle, 2017).

47

48 Developmental factors and pathways co-opted by cancers are often related to vital
49 cellular functions, such as proliferation, migration, and differentiation (Caramel et al.,
50 2013; Casas et al., 2011; McConnell et al., 2019; Perego et al., 2018). Furthermore, the
51 embryonic origin of specific tissues can impact the aggressive phenotypes tumors are

52 able to acquire (Carreira et al., 2006; Gupta et al., 2005; Hoek & Goding, 2010). In the
53 case of melanoma, the cell of origin, the melanocyte, is derived from the neural crest, a
54 highly migratory population of embryonic cells. Thus, melanomas are prone to early and
55 aggressive metastasis, associated with the expression of neural crest migratory factors
56 (Liu, Fukunaga-Kalabis, Li, & Herlyn, 2014). Additionally, melanomas lacking
57 differentiation exhibit more aggressive characteristics and are broadly more resistant to
58 therapy (Fallahi-Sichani et al., 2017; Knappe et al., 2016; Landsberg et al., 2012; Mehta
59 et al., 2018; Muller et al., 2014; Shaffer et al., 2017; Zuo et al., 2018). While
60 differentiation status is evidently important in the course of disease, the mechanisms by
61 which melanomas and other cancers remain less differentiated are poorly understood.
62 Since many of the factors associated with a lack of differentiation in these cancers are
63 expressed and apparently function during embryogenesis, elucidating the
64 developmental roles of these factors can give insight into their behaviors and roles in
65 tumorigenesis and progression.

66

67 A key pathway involved in early development and development of the neural crest is the
68 bone-morphogenetic protein (BMP) pathway (reviewed in Kishigami & Mishina, 2005).
69 The BMP pathway is activated by BMP-ligands binding to BMP receptors, which can
70 then phosphorylate SMAD1, SMAD5, and SMAD8 (also called SMAD9).
71 Phosphorylated SMAD1/5/8 associates with co-SMAD4, forming a complex that can
72 translocate to the nucleus and regulate expression of target genes. BMP signaling is
73 important in early embryonic dorsoventral patterning and induction of the neural crest
74 (Garnett, Square, & Medeiros, 2012; Hashiguchi & Mullins, 2013; McMahon et al., 1998;

75 Schumacher, Hashiguchi, Nguyen, & Mullins, 2011). Following neural crest induction,
76 BMP signaling has been implicated in patterning within the neural crest and surrounding
77 tissues, as well as development of nervous system- and musculoskeletal-related neural
78 crest lineages (Hayano, Komatsu, Pan, & Mishina, 2015; McMahon et al., 1998;
79 Nikaido, Tada, Saji, & Ueno, 1997; Reichert, Randall, & Hill, 2013; Valdivia et al., 2016).
80 While many developmental functions of BMP signaling are well characterized, the
81 relationship of BMP signaling to the development of pigment cells from the neural crest
82 is poorly understood.

83

84 Our laboratory recently identified a BMP ligand, *GDF6*, that acts to suppress
85 differentiation and cell death in melanoma (Venkatesan et al., 2018). We found that
86 *GDF6*-activated BMP signaling in melanoma cells represses expression of *MITF*, a key
87 regulator of melanocyte differentiation, leading to a less differentiated state. Here, we
88 investigate the role of *GDF6* and the BMP pathway in development of pigment cells in
89 zebrafish. We show that BMP signaling regulates fate specification of neural crest-
90 derived pigment cell lineages and suppresses expression of *mitfa*, an ortholog of *MITF*.
91 Furthermore, we show that disrupting BMP signaling alters fate specification between
92 melanocyte and iridophore populations in the zebrafish. We determine that this shift in
93 fate occurs at the level of an *mitfa*-positive pigment progenitor cell, and that BMP
94 signaling acts through *mitfa* to direct *mitfa*-positive pigment progenitor cells to a specific
95 fate. Altogether, these findings suggest pathologic BMP signaling in melanoma is a
96 reiteration of normal physiologic function of BMP signaling during melanocyte
97 development.

98

99 **Results**

100

101 **Loss of *gdf6a* leads to an increase in adult pigmentation**

102 To understand potential functions of *gdf6a* in the melanocyte lineage, we first
103 determined if any alterations in pigment pattern were present in animals lacking *gdf6a*.
104 In these studies, we used the *gdf6a*^{s327} allele, hereafter referred to as *gdf6a(lf)*, which
105 encodes an early stop codon and has previously been shown to cause a complete loss
106 of *gdf6a* function (Gosse & Baier, 2009). Previous studies have identified early roles for
107 *gdf6a* during initial embryonic patterning, including dorsoventral patterning immediately
108 following fertilization, thus *gdf6a(lf)* mutants have significantly decreased viability during
109 the first 5 days post fertilization (Sidi, Goutel, Peyrieras, & Rosa, 2003). However, we
110 found that a small proportion of *gdf6a(lf)* animals are able to survive early development
111 and progress to adulthood. These *gdf6a(lf)* adult zebrafish had increased pigmentation
112 when compared to wild-type zebrafish (Figure 1A). Furthermore, *gdf6a(lf)* adult
113 zebrafish had qualitative disruption of the normal pigment pattern of both stripe and
114 scale-associated melanocytes, and a significant increase in the number of scale-
115 associated melanocytes as well as the overall scale area covered by melanin (Figure
116 1A,1B). These results indicate that *gdf6a(lf)* mutants have melanocyte defects.

117

118 **Loss of *gdf6a* or inhibition of BMP signaling leads to an increase in embryonic**
119 **melanocytes**

120 Since zebrafish develop their adult pigment pattern during metamorphosis, it is possible
121 *gdf6a* acts during this stage to change adult pigmentation, and not during initial pigment

122 cell development in embryogenesis (D. M. Parichy & Spiewak, 2015; Patterson &
123 Parichy, 2013; Quigley et al., 2004). To address this issue, we investigated whether
124 *gdf6a(lf)* caused embryonic pigmentation changes and, if so, whether any such changes
125 were BMP-dependent. We crossed *gdf6a(lf)* heterozygotes and, in randomly selected
126 progeny, quantified the number of melanocytes that developed by 5 days post-
127 fertilization (DPF). Following melanocyte quantification, we determined the genotype of
128 each embryo. In parallel, we treated wild-type zebrafish during the period of neural crest
129 induction and melanocyte specification (12 to 24 hours post fertilization) with a small
130 molecule BMP inhibitor, DMH1, hereafter referred to as BMPi, and performed the same
131 quantification of embryonic melanocytes (Hao et al., 2010). *gdf6a(lf)* homozygous
132 animals developed approximately 40% more dorsal melanocytes by 5 DPF, when
133 compared to sibling wild-type animals and *gdf6a(lf)* heterozygotes (Figures 1C,1D and
134 S1A). *gdf6a(lf)* animals also showed increased expression of *tyrp1b*, a marker of
135 differentiated melanocytes, which is consistent with an increase in melanocyte number
136 (Figure 1E). Furthermore, treatment with BMPi phenocopied the melanocyte changes
137 observed in *gdf6a(lf)* mutants, coupled with a similar increase in expression of *tyrp1b*
138 (Figures 1D and 1E). We observed a similar increase in total body melanocytes,
139 indicating that there is an overall increase in melanocyte development instead of a
140 failure of migration leading to a specific increase in dorsal melanocytes (Figure S1B).
141 These results indicate *gdf6a*-activated BMP signaling normally acts in embryos to limit
142 melanocyte development.

143

144 *gdf6* ortholog expression during neural crest development

145 Numerous BMP ligands are expressed during early embryogenesis and participate in
146 multiple facets of development, including neural crest induction. It was previously shown
147 that multiple BMP ligands are activated during zebrafish neural crest development
148 (Reichert et al., 2013). Of those ligands investigated, only *gdf6a* and *bmp6* were
149 expressed in the neural crest, and only *gdf6a* activated BMP signaling within neural
150 crest cells. An additional study identified dorsal expression of a zebrafish paralog of
151 *gdf6a*, *gdf6b*, indicating it could potentially act in the neural crest (Bruneau & Rosa,
152 1997). We verified *gdf6b* expression is restricted to the neural tube, and further
153 determined *gdf6b* loss of function has no impact on pigment cell development by
154 generating a *gdf6b* mutant, hereafter referred to as *gdf6b(lf)*, and counting embryonic
155 melanocytes (Figure S1D, S1E, S1F and S1G). We generated double mutants for both
156 *gdf6a(lf)* and *gdf6b(lf)* to assess whether these paralogs functioned redundantly or could
157 compensate for the loss of one another. Unfortunately, *gdf6a(lf)*; *gdf6b(lf)* double
158 mutants had significant morphologic defects and decreased viability such that we could
159 not adequately compare melanocyte numbers in these animals (Figure S1H and S1I).
160 However, because there were no pigmentation defects in *gdf6b(lf)* mutants and *gdf6a(lf)*
161 pigmentation defects were the same severity as observed in animals treated with a pan-
162 BMP inhibitor, it is likely that most, if not all, effects of BMP signaling on melanocyte
163 development are directed by *gdf6a*.

164

165 BMP inhibition increases *mitfa*-positive pigment cell progenitors in the neural crest

166 We sought to determine the mechanism by which BMP signaling inhibits melanocyte
167 development in embryos. Based on our experiments using BMPi, we suspected BMP

168 signaling acts during pigment cell development from the neural crest to prevent an
169 increase in melanocytes. Following induction, neural crest cells undergo proliferation,
170 followed by fate restriction and specification, in which individual cells become less and
171 less multipotent until a single possible fate remains (Jin, Erickson, Takada, & Burrus,
172 2001; Lewis et al., 2004; Nagao et al., 2018). In many cases, specification to the
173 ultimate lineage is determined by activation of an individual or a group of lineage-
174 specific factors (Sauka-Spengler, Meulemans, Jones, & Bronner-Fraser, 2007). For
175 pigment cells, fate specification is dependent on integration of many signaling factors,
176 including BMP and Wnt signaling, as well as key transcription factors, such as SOX-,
177 *PAX*-, and *FOX*-family transcription factors (Garnett et al., 2012; Ignatius, Moose, El-
178 Hodiri, & Henion, 2008; Lister et al., 2006; Sato, 2005; Southard-Smith, Kos, & Pavan,
179 1998; Thomas & Erickson, 2009). In zebrafish, specification of the pigment cell lineage
180 depends on upregulation of *sox10* and downregulation of factors inhibiting
181 differentiation, such as *foxd3* (Curran et al., 2010; Curran, Raible, & Lister, 2009; Dutton
182 et al., 2001). Following *sox10* upregulation, a subset of *sox10*-positive cells can activate
183 pigment lineage markers associated with melanocytes, iridophores, and xanthophores
184 (Elworthy, Lister, Carney, Raible, & Kelsh, 2003; Fadeev, Krauss, Singh, & Nusslein-
185 Volhard, 2016; Nagao et al., 2018; Nord, Dennhag, Muck, & von Hofsten, 2016;
186 Petratou et al., 2018). *mitfa* is a key factor that is expressed early in pigment progenitor
187 cells (Lister, Robertson, Lepage, Johnson, & Raible, 1999). Based on this framework,
188 we hypothesized two potential mechanisms by which supernumerary melanocytes are
189 generated: 1) an increase in proliferation of either neural crest cells or pigment
190 progenitor cells, or 2) an increase in the proportion of neural crest cells that are

191 specified to become pigment progenitor cells. To assess changes in proliferation of
192 neural crest cells and pigment cells, we analyzed cell cycle profiles using flow
193 cytometry. Embryos expressing reporters for neural crest cells (*Tg(crestin:eGFP)*) or
194 pigment progenitor cells (*Tg(mitfa:eGFP)*) were treated with BMPi from 12 to 24 HPF,
195 during neural crest development and specification (Curran et al., 2009; Kaufman et al.,
196 2016). Embryos were dissociated, stained with DAPI, and analyzed for DNA content of
197 neural crest cells or pigment progenitor cells as defined by the fluorescent GFP marker
198 (Figure S2A). We observed no increase in the percent of S/G2/M cells in either
199 population, indicating no apparent change to proliferation in either neural crest cells or
200 pigment progenitor cells (Figure S2B, S2C). Without an obvious increase in
201 proliferation, we tested the hypothesis that a change in specification results in increased
202 melanocytes. To assess changes in specification of neural crest cells into pigment
203 progenitor cells, we utilized reporter embryos marking neural crest cells in red
204 (*Tg(crestin:mCherry)*) and pigment progenitor cells in green (*Tg(mitfa:eGFP)*) (Figure
205 2A). Using these reporters, neural crest cells not committed to the pigment cell lineage
206 are *crestin:mCherry* single-positive, whereas *crestin:mCherry/mitfa:eGFP* double-
207 positive cells are those newly committed to the pigment cell lineage. We treated
208 embryos containing both reporter transgenes with BMPi from 12 to 24 HPF, during
209 neural crest development and specification. At 24 HPF, we dissociated embryos and
210 analyzed cells for fluorescent marker expression by flow cytometry (Figure 2A).
211 Embryos treated with BMPi showed approximately a 1.5-fold increase in the percentage
212 of *crestin:mCherry/mitfa:eGFP* double-positive cells per total *crestin:mCherry*-positive
213 cells (Figure 2B, 2C). We further verified a change in specification by staining BMPi- or

214 vehicle-treated *Tg(crestin:eGFP)* embryos with anti-Mitfa antibody and assessed the
215 proportion of *crestin:eGFP*-positive cells that stained positive for Mitfa (Figure 2D). We
216 observed a 1.3-fold increase in the proportion of Mitfa/*crestin:eGFP* double-positive
217 cells per total *crestin:eGFP*-positive cells in animals treated with BMPi compared to
218 vehicle control (Figure 2E). Altogether these results suggest that an increase in
219 embryonic melanocytes is caused by an increase in the proportion of neural crest cells
220 specified as pigment progenitor cells, rather than a change in proliferation of either
221 neural crest or pigment progenitor cells.

222

223 BMP signaling in *mitfa*-expressing pigment progenitor cells can alter melanocyte
224 development in embryogenesis

225 Because we observed an impact of BMP signaling on neural crest-to-pigment progenitor
226 cell specification, we explored the relationship between *gdf6a* and *mitfa* expression. We
227 performed *in situ* hybridization for *gdf6a* and *mitfa* during the course of neural crest and
228 melanocyte development (Figure 3A). As described previously (Reichert et al., 2013;
229 Rissi, Wittbrodt, Délot, Naegeli, & Rosa, 1995), *gdf6a* is expressed in the neural crest
230 during induction. We observe downregulation of *gdf6a* in a rostrocaudal fashion as
231 development proceeds. *mitfa* is expressed inversely, being turned on in neural crest
232 cells rostrocaudally in the zone vacated by *gdf6a*. The timing of *gdf6a* and *mitfa*
233 expression changes is consistent with the possibility that *gdf6a*-driven BMP signaling
234 acts in neural crest cells to repress *mitfa* expression and prevent excess pigment
235 progenitor cells from being specified. However, we also considered the possibility that
236 BMP signaling is active in *mitfa*-positive cells and affects the fates of these cells. To

237 determine if BMP signaling is active in *mitfa*-positive cells, we stained *Tg(mitfa:eGFP)*
238 zebrafish with antibodies against phosphorylated-SMAD-1/5/8 (pSMAD). We verified
239 specificity of the anti-pSMAD antibody using BMPi treated embryos (Figure S3). 30% of
240 *mitfa*-expressing cells on the leading, caudal edge of the *mitfa* expression domain had
241 nuclear-localized pSMAD staining, whereas only 7% of *mitfa*-expressing cells in regions
242 rostral to the leading edge showed nuclear pSMAD staining (Figure 3B and 3C). These
243 results suggest BMP signaling is active as *mitfa*-expressing cells first arise in the neural
244 crest, but is turned off in such cells as development proceeds. To assess if BMP activity
245 in *mitfa*-expressing cells can impact melanocyte development, we directly altered BMP
246 activity in these cells. We first generated a stably transgenic zebrafish line expressing
247 *gdf6a* under the control of the *mitfa* promoter (*Tg(mitfa:gdf6a)*) to increase *gdf6a*
248 expression in *mitfa*-expressing cells. Embryos expressing the *Tg(mitfa:gdf6a)* transgene
249 developed fewer melanocytes than non-transgenic sibling controls (Figure 4A). To alter
250 BMP signaling in a cell-autonomous manner within *mitfa*-expressing cells, we used the
251 miniCoopR system in two complementary approaches: a) to express a dominant
252 negative BMP receptor (dnBMPR), which suppresses intracellular BMP activity, and b)
253 to express a phospho-mimetic variant of SMAD1 (SMAD1-DVD) to constitutively
254 activate intracellular BMP activity (Ceol et al., 2011; Nojima et al., 2010; Pyati, Webb, &
255 Kimelman, 2005). We injected *mitfa(lf)* animals with miniCoopR-dnBMPR, miniCoopR-
256 SMAD1-DVD, or control miniCoopR-eGFP (Figure 4B). At 5 DPF, we scored animals for
257 rescue of melanocytes. Animals injected with miniCoopR-dnBMPR showed a rescue
258 rate of 79% as compared to 29% of miniCoopR-eGFP-injected animals. Furthermore,
259 animals injected with miniCoopR-SMAD1-DVD showed a 15% rescue rate (Figure 4C).

260 Together these results suggest BMP signaling is active in *mitfa*-expressing cells and
261 modulating BMP signaling can alter the fate of these *mitfa*-expressing cells during
262 development. Thus, *gdf6a*-driven BMP signaling can both limit the number of *mitfa*-
263 expressing cells arising from the neural crest but also act in *mitfa*-expressing pigment
264 progenitor cells to influence their development into melanocytes.

265

266 Iridophores, but not other neural crest derivatives, are reduced upon *gdf6a* loss

267 Because we observed no change in proliferation of *crestin*- or *mitfa*-positive
268 populations, but the number of melanocytes developing from these precursors was
269 increased, we questioned whether this increase corresponded with a commensurate
270 loss of a related pigment or other neural crest-derived cell type. To determine what cells
271 may be impacted, we looked for transcriptional changes in markers of other, related
272 neural crest derivatives. We isolated RNA from *gdf6a(lf)* and wild-type embryos at 5
273 DPF. Additionally, we isolated RNA from embryos treated with a BMPi or vehicle
274 control. We performed qPCR for markers of neural crest derivatives, including *mbpa* for
275 glial cells, *pomca* for adrenal medullary cells, *neurog1* for neuronal cells, *aox5* for
276 xanthophores, and *pnp4a* for iridophores (Fadeev et al., 2016; McGraw, Nechiporuk, &
277 Raible, 2008; D.M. Parichy, Ransom, Paw, Zon, & Johnson, 2000; Thomas & Erickson,
278 2009). As a control, we used a chondrocyte marker, *col2a1a*, as craniofacial
279 development has previously been described to be disrupted by *gdf6a* loss (Reed &
280 Mortlock, 2010). Per our previous analysis, *gdf6a(lf)* mutants demonstrated an increase
281 in expression of the melanocyte marker *tyrp1b* (Figure 1E). And as predicted based on
282 previous literature, *gdf6a(lf)* mutants showed a decrease in expression of the

283 chondrocyte marker, *col2a1a*. Markers for neuronal, glial, adrenal medullary, and
284 xanthophore lineages were no different in *gdf6a* compared to wild-type animals (Figure
285 5A). Similar results were obtained in animals treated with a BMPi, with the exception of
286 a change in *mbpa* expression, a marker for glial cells. Previous studies have shown glial
287 cell development is regulated in part by BMP activity (Jin et al., 2001). Since *mbpa*
288 expression was unchanged in *gdf6a(lf)* animals, this suggests another BMP ligand is
289 involved in activating BMP signaling to promote glial cell development. For neuronal and
290 xanthophore cell populations, we verified that the expression profile correlated with cell
291 numbers or development of key structures. We treated animals with BMPi or vehicle
292 and stained with anti-HuC/D antibody to label neuronal cells in the dorsal root ganglia
293 and developing gastrointestinal tract (Lister et al., 2006) (Figure S4A-C). We detected
294 no difference in dorsal root ganglia and enteric neuron development between each
295 group. We imaged animals stably expressing *Tg(aox5:PALM-eGFP)* to label
296 xanthophores and found no qualitative difference in xanthophores between BMPi- and
297 vehicle-treated groups (Eom & Parichy, 2017) (Figure S4D). In our transcriptional
298 analyses of *gdf6a(lf)* and BMPi-treated embryos, we observed a decrease in expression
299 of *pnp4a*, a marker for the iridophore lineage, indicating a potential deficit of iridophore
300 development (Figure 5A). Since *pnp4a* is expressed in other developing cells and
301 tissues, such as retinal cell populations, we wanted to confirm these changes were
302 specific to a deficit in neural crest-derived body iridophores (Cechmanek & McFarlane,
303 2017; Lopes et al., 2008; Petratou et al., 2018). We quantified the number of dorsal
304 iridophores that developed in *gdf6a(lf)* embryos (Figure 5B) and embryos treated with
305 BMPi (Figure 5C) at 5 DPF, using incident light to highlight embryonic iridophores.

306 Embryos developed 32% and 27% fewer iridophores with *gdf6a(lf)* or BMPi treatment,
307 respectively. Together, these results indicate that *gdf6a*-driven BMP signaling promotes
308 iridophore development.

309

310 BMP inhibition increases the likelihood a multipotent precursor will develop into a
311 melanocyte

312 Melanocytes and iridophores have previously been shown to develop from *mitfa*-
313 expressing pigment progenitor cells (Curran et al., 2010; Curran et al., 2009). To
314 determine if BMP signaling regulates fate specification of melanocytes and iridophores
315 from *mitfa*-expressing pigment progenitor cells, we performed lineage tracing. We
316 injected *Tg(ubi:switch)* embryos, which stably express a *ubi:loxP-GFP-STOP-loxP*-
317 *mCherry-STOP* transgene (Mosimann et al., 2011) with a *mitfa:Cre-ERT2* transgene to
318 generate mosaic expression of Cre-ERT2 in *mitfa*-positive cells (Figure 6A). Injected
319 embryos were treated with BMPi and hydroxytamoxifen (4-OHT), the latter to allow
320 nuclear localization of Cre and generate recombinant events in individual *mitfa*-
321 expressing pigment progenitor cells. Since these *mitfa*-expressing pigment progenitor
322 cells are transient, 4-OHT treatment was limited to 12 to 24 HPF, with thorough fish
323 water exchange to wash out the drug and prevent recombinant events after
324 specification. At 5 DPF, embryos with individual recombinant events, indicated by single
325 mCherry-positive cells, were evaluated for the fate of those cells. In animals treated with
326 BMPi, we observed an increase in the ratio of labeled melanocytes to iridophores as
327 compared to vehicle-treated controls (Figure 6B, S5). This result suggests that BMP

328 signaling normally promotes the development of *mitfa*-expressing pigment progenitor
329 cells into iridophores at the expense of melanocytes.

330

331 BMP signaling represses *mitfa* expression within neural crest and pigment progenitor
332 cells

333 Previous studies have indicated that the expression level of *mitfa* within pigment
334 progenitor cells is important in specifying a melanocyte versus iridophore fate (Curran et
335 al., 2010; Curran et al., 2009). Cells with a higher level *mitfa* expression are more likely
336 to become melanocytes, while those that downregulate *mitfa* are more likely to become
337 iridophores. Since *gdf6a(lf)* and BMP-inhibited embryos have excess melanocytes and
338 fewer iridophores, we hypothesized that this phenotype resulted from disrupted
339 regulation of *mitfa* expression in these embryos. This hypothesis was driven, in part, by
340 our previous data in human melanoma cells, in which knockdown of *GDF6* decreased
341 phospho-SMAD1/5/8 binding at the *MITF* promoter and increased *MITF* expression
342 (Venkatesan et al., 2018). To assess *mitfa* levels within neural crest cells and *mitfa*-
343 expressing pigment progenitor cells, we treated *Tg(crestin:eGFP)* and *Tg(mitfa:eGFP)*
344 embryos with BMPi as previously described. We dissociated embryos and used
345 fluorescence-activated cell sorting (FACS) to isolate *crestin-eGFP*-positive or
346 *mitfa:eGFP*-positive cells. We then assessed *mitfa* transcript levels in each population
347 by qPCR. Treatment with BMPi led to approximately 3-fold and 6-fold increases in *mitfa*
348 expression in *crestin:eGFP*-positive and *mitfa:eGFP*-positive cells, respectively (Figure
349 7A). To explore this question on a single-cell level and analyze Mitfa protein levels, we
350 stained BMPi-treated and vehicle-treated *Tg(crestin:eGFP)* embryos with an anti-Mitfa

351 antibody (Figure 7B) (Venkatesan et al., 2018). In BMPi-treated animals, we observed a
352 2.5-increase in Mitfa staining intensity in *crestin:eGFP*-positive cells, indicating inhibition
353 of BMP signaling leads to an increase in Mitfa protein in pigment progenitor cells at a
354 single-cell level (Figure 7C). Furthermore, those cells that were Mitfa-positive and
355 *crestin:eGFP*-negative showed a 1.7-fold increase in Mitfa staining intensity, indicating
356 inhibition of BMP signaling also leads to an increase in Mitfa protein following
357 specification of pigment cells (Figure 7B, 7C). Together, these results indicate BMP
358 signaling suppresses *mitfa* expression in cells during specification of pigment cell
359 lineages.

360

361 Regulation of pigment cell fate by BMP signaling is dependent on *mitfa*

362 If deregulated *mitfa* expression is critical to the phenotypic defects observed upon
363 inhibition of BMP signaling, then these defects should be dependent on *mitfa* function.
364 To determine whether *mitfa* is indeed responsible for mediating the shift in cell fate
365 regulated by BMP activity, we treated *mitfa(lf)* embryos with BMPi. As *mitfa* is necessary
366 for the specification of all body melanocytes, *mitfa(lf)* animals do not develop any
367 melanocytes during embryogenesis or through adulthood. However, these animals can
368 develop iridophores and develop a greater number of iridophores at baseline than their
369 wild-type counterparts (Lister et al., 1999). We hypothesized that, if an elevation of *mitfa*
370 expression in BMPi-treated embryos was required to shift pigment progenitor cell fates
371 from iridophores to melanocytes, there would be no decrease in the number of
372 iridophores when *mitfa(lf)* embryos were treated with BMPi. Indeed, BMPi-treated
373 embryos showed no difference in the number of iridophores compared to vehicle-

374 treated controls (Figure 7D, 7E). Together, these results indicate that BMP inhibition
375 requires *mitfa* to direct pigment progenitor cells away from iridophore fate.

376

377 **Discussion**

378 Our results elucidate a role for *gdf6a*-activated BMP signaling in suppressing
379 melanocyte development from the neural crest during embryogenesis. Inhibition of BMP
380 signaling leads to an increase of neural crest cells expressing *mitfa*, affecting the
381 proportion of neural crest cells specified as pigment progenitor cells. Additionally, in
382 BMP-inhibited embryos these *mitfa*-positive pigment progenitor cells demonstrate an
383 increased propensity to become melanocytes, instead of iridophores. Cells in BMP-
384 inhibited embryos have increased expression of *mitfa*, and the function of *mitfa* is
385 required for the reduction of iridophores observed in BMP-inhibited embryos. Based on
386 these findings, we propose that *gdf6a*-activated BMP signaling normally represses *mitfa*
387 expression, limiting both the development of pigment progenitor cells from the neural
388 crest and the specification of melanocytes from these pigment progenitor cells. As
389 discussed below, *MITF* is downregulated by *GDF6*-activated BMP signaling to prevent
390 melanocytic differentiation in melanomas (Venkatesan et al., 2018). The function we
391 have defined for *gdf6a*-activated BMP signaling in development suggests that its activity
392 is co-opted in tumors to prevent differentiation of melanoma cells.

393

394 **Regulation of pigment cell fate by BMP signaling**

395 Our studies indicate *gdf6a*-activated BMP signaling can regulate pigment cell
396 development from the neural crest in two ways. First, BMP signaling restricts the

397 number of neural crest cells that transition into *mitfa*-positive pigment cell progenitors.

398 When BMP signaling is abrogated, additional cells adopt a pigment progenitor fate,

399 which likely is a source of supernumerary melanocytes. Second, BMP signaling biases

400 the fate choice of *mitfa*-positive progenitor cells. In BMP-deficient embryos, *mitfa*-

401 positive progenitor cells more often become melanocytes and less often become

402 iridophores. Previous studies have suggested a common melanocyte-iridophore

403 progenitor (Curran et al., 2010; Curran et al., 2009; Petratou et al., 2018), and our data

404 support the existence of such a progenitor and indicate that it is *mitfa*-expressing and

405 influenced by BMP signaling. While BMP signaling regulates the fate of a common

406 melanocyte-iridophore precursor, the decrease in the number of iridophores cannot fully

407 account for the number of melanocytes gained in *gdf6a(lf)* and BMPi-treated embryos.

408 Because *gdf6a(lf)* and BMPi-treatment are potentially impacting the entirety of neural

409 crest development, other neural crest cells may be mis-specified to the melanocyte

410 lineage. This misspecification could account for the discrepancy between the gain of

411 melanocytes and loss of iridophores. If misspecification of other neural crest cells is

412 occurring, other neural crest lineages could show a deficit. However, in our assays

413 evaluating other lineages, we detected no deficits outside of a loss of iridophores.

414 Among several possibilities, the deficit may be present in a neural crest lineage we did

415 not directly measure. Alternatively, deficits in other neural crest lineages may be small

416 and distributed across multiple other lineages, such that our assays are unable to detect

417 those subtle changes. Lastly, proliferation within the neural crest and of neural crest

418 derivatives following migration from the crest is known to occur (Dougherty et al., 2013;

419 Gianino, Grider, Cresswell, Enomoto, & Heuckerth, 2003), and it is possible that such

420 proliferation could compensate for any deficit. In summary, the supernumerary
421 melanocytes observed in *gdf6a(lf)* and BMPi-treated embryos are likely to arise from
422 some combination of neural crest cells that are shunted to the pigment cell lineage and
423 melanocyte-iridophore precursors that preferentially adopt a melanocyte fate.

424

425 Regulation of *mitfa* by BMP signaling

426 Our studies identify *gdf6a*-activated BMP signaling as a regulator of *mitfa* during
427 pigment cell development in zebrafish. Previous studies have identified roles for *gdf6a*
428 in the preplacodal ectoderm, retinal cell survival, and craniofacial development in
429 zebrafish, while others have broadly connected BMP signaling to fate determination and
430 cell survival in the neural crest in other model systems (French, Erickson, French,
431 Pilgrim, & Waskiewicz, 2009; Gosse & Baier, 2009; Hanel & Hensey, 2006; Jin et al.,
432 2001; Reed & Mortlock, 2010; Reichert et al., 2013). However, the specific role of BMP
433 signaling and of *gdf6a* on pigment cell development has heretofore been
434 uncharacterized. Our analyses indicate that *gdf6a* is expressed in neural crest cells
435 prior to the rostrocaudal onset of *mitfa* expression. In addition, we observed an overlap
436 of BMP activity and *mitfa* expression at the leading edge of the rostrocaudal *mitfa*
437 progression. When BMP signaling was inhibited, we found increased expression in
438 neural crest cells of *mitfa* RNA and Mitfa protein. Together, these results suggest that
439 *gdf6a*-driven BMP signaling regulates expression of *mitfa* and, consequently, directs
440 fates adopted by *mitfa*-expressing cells. We speculate that such a role underlies the
441 excess melanocytes observed in *gdf6a(lf)* and BMPi-treated embryos. In the absence of
442 *gdf6a* and BMP signaling, increased expression of *mitfa* could lead to a greater

443 proportion of neural crest cells adopting a pigment cell fate and could lead to a greater
444 propensity of melanocyte-iridophore precursors adopting a melanocyte fate. These
445 findings are consistent with what has previously been established in human melanoma
446 cells, where *GDF6*-activated BMP signaling has been shown to promote pSMAD
447 binding to *MITF* and is suspected to directly regulate *MITF* expression (Venkatesan et
448 al., 2018). Our results support this regulatory role and provide a developmental context
449 *in vivo* to understand why *GDF6*-activated BMP signaling is able to regulate *MITF* in
450 melanoma cells.

451

452 Reiteration of normal physiologic function in melanoma

453 *GDF6* and BMP signaling were previously described in melanoma to suppress
454 differentiation through binding of pSMAD to *MITF* and corresponding repression of *MITF*
455 expression (Venkatesan et al., 2018). Results from the current study indicate *gdf6a* and
456 BMP signaling likely act in a similar fashion during development to repress expression
457 of *MITF*, either directly or indirectly, leading to suppression of melanocyte specification
458 and differentiation from the neural crest. Together, these findings suggest BMP activity
459 in melanoma is a recapitulation of normal regulatory functions executed by *gdf6a* and
460 BMP signaling during pigment cell development. It has been previously established that
461 lineage programs can be co-opted by cancers to promote pro-tumorigenic
462 characteristics (Carreira et al., 2006; Gupta et al., 2005). These programs activate EMT
463 factors, such as *TWIST1* and *SNAI2*, and factors associated with neural crest
464 multipotency, such as *SOX10*, to promote invasiveness, proliferative capacity,
465 metastatic capability, and therapeutic resistance (Caramel et al., 2013; Casas et al.,

466 2011; Shakhova et al., 2015). However, it is unclear if these factors have similar
467 regulation between normal development and melanoma. Here, we have described a
468 developmental role for *GDF6* that is reiterated in a pathologic process in disease.
469 Because initiation and maintenance of neural crest gene expression has been shown to
470 be important in melanoma, a better understanding of how regulation occurs during
471 development may have clinical implications (Kaufman et al., 2016). Our findings indicate
472 BMP signaling has a regulatory role over key differentiation genes during melanocyte
473 development from the neural crest. Many studies have implicated expression of neural
474 crest and melanocyte factors during many phases of melanoma, including initiation,
475 progression, invasion, metastasis, and therapeutic resistance of melanoma (Carreira et
476 al., 2006; Fallahi-Sichani et al., 2017; Gupta et al., 2005; Kaufman et al., 2016; Shaffer
477 et al., 2017). Taken together, these findings suggest therapeutic targeting of *GDF6* or
478 BMP signaling would likely have a positive impact on prognosis and outcome in
479 melanoma patients by promoting differentiation in tumors.

480

481 **Acknowledgements**

482 We thank Nathan Lawson for *pcsDest2* plasmid; David Kimelman for the *dnBMPR*
483 plasmid; Takenobu Katagiri for the *SMAD1-DVD* plasmid; Christian Mossiman for
484 *Tg(ubi:switch)* zebrafish strain and *CreERT2* plasmid; Charles Kaufmann for
485 *Tg(crestin:eGFP)* and *Tg(crestin:mCherry)* zebrafish strains; Patrick White, Ed Jaskolski
486 and the staff at the UMMS Animal Medicine Department for fish care; Tammy Krumpoch
487 for guidance and assistance in performing flow cytometry and FACS experiments. AKG
488 was supported by a Melanoma Research Foundation Looney Legacy Foundation

489 Medical Student Award, Center for Translational Sciences TL1 Training Fellowship
490 through the UMMS CCTS (UL1-TR001453), NCI NRSA F31 Predoctoral Fellowship
491 (1F31CA239478-01). Research was supported by a Kimmel Scholar Award (SKF-13-
492 123), Department of Defense Peer Reviewed Cancer Research Program Career
493 Development Award (W8IXWH-13-0107) and NIH National Institute of Arthritis and
494 Musculoskeletal and Skin Diseases grant (R01AR063850) to CJC. The content is solely
495 the responsibility of the authors and does not necessarily represent the official views of
496 the Department of Defense or NIH.

497

498 **Author Contributions**

499 AKG, AMV, and CJC conceived the project. AKG, AMV, and CJC designed and
500 interpreted the melanocyte quantification experiments and results. AKG and CJC
501 designed and interpreted the proliferation, specification, and neural crest lineage
502 experiments and results. AKG performed the flow cytometry, qPCR,
503 immunofluorescence, lineage tracing and *in situ* hybridization experiments. AKG and
504 AMV performed the melanocyte quantification experiments. AMV generated the
505 MiniCoopR and pCS-DEST plasmids and generated the probes for *in situ* hybridization.
506 AMV and MG generated and isolated *gdf6b* mutant zebrafish. AKG and CJC wrote the
507 manuscript.

508

509 **Declaration of Interests**

510 The authors declare no competing interests.

511

512 **Methods**

513 **Zebrafish**

514 Zebrafish were handled in accordance with protocols approved by the University of
515 Massachusetts Medical School IACUC. Fish stocks were maintained in an animal
516 facility at 28.5°C on a 14-hour/10-hour Light/Dark cycle (Westerfield, 1995). The wild-
517 type strain used was AB. Published strains used in this study include *gdf6a(lf)*
518 (*gdf6a*^{s327}) (Gosse & Baier, 2009), *Tg(mitfa:eGFP)* (Curran et al., 2009),
519 *Tg(crestin:eGFP)* (Kaufman et al., 2016), *Tg(crestin:mCherry)* (Kaufman et al., 2016),
520 *mitfa(lf)* (Lister et al., 1999), *Tg(ubi:switch)* (Mosimann et al., 2011), *Tg(aox5:PALM-*
521 *eGFP*) (Eom & Parichy, 2017). Construction of new strains generated are detailed
522 below.

523

524 **DNA Constructs**

525 DNA constructs were built using Gateway cloning (Life Technologies). Sequences of
526 *gdf6a*, *dnBMPR* (Pyati et al., 2005) and *SMAD1-DVD* (Nojima et al., 2010) were PCR-
527 amplified and cloned into pDONR221 (Life Technologies). Oligonucleotides used in
528 cloning are described in Key Resources Section. Previously published entry clones
529 used in this study were pENTRP4P1r-*mitfa* (Ceol et al., 2011), pDONR221-*gdf6b*
530 (Venkatesan et al., 2018), pDONR221-*CreERT2* (Mosimann et al., 2011). Previously
531 published destination vectors used in this study are MiniCoopR (MCR) (Ceol et al.,
532 2011) and pcsDest2 (Villefranc, Amigo, & Lawson, 2007). p3E-*polyA*, pME-*eGFP*,
533 pDestTol2CG2, pDestTol2pA2, pCS2FA-transposase were acquired from the Tol2Kit
534 (Kwan et al., 2007). Using the entry clones and destination vectors described above, the

535 following constructions were built using multisite or single site Gateway (Life
536 Technologies): MCR-mitfa:dnBMPR:pA, MCR-mitfa:eGFP:pA, MCR-mitfa:SMAD1-
537 DVD:pA, pDestTol2CG2-mitfa:gdf6a:pA, pDestTol2pA2-mitfa:CreERT2:pA, pcsDest2-
538 gdf6a, pcsDest2-gdf6b. All constructs were verified by restriction digest or sequencing.

539

540 Construction of *gdf6b(lf)*

541 To generate *gdf6b(lf)* mutants, we used TALEN genome editing. TALEN's were
542 designed targeting exon 1 of *gdf6b* (TAL1 sequence: GTCAGCATCACTGTTAT; TAL2
543 sequence: CCTTGATCGCCCTTCT). TALENs were assembled using the Golden Gate
544 TALEN kit (Addgene) per the manufacturer's instructions. TALEN plasmids were
545 linearized and transcribed with mMESSAGE mMACHINE kit (Ambion). Zebrafish
546 embryos were injected with 50 pg of mRNA of each TALEN arm. Injected embryos (F0)
547 were matured to breeding age and outcrossed. Resulting offspring (F1) were genotyped
548 by extraction genomic DNA from fin clips per standard protocol and PCR amplification
549 with *gdf6b* primers. F1 offspring carrying mutations by genotyping were sequenced to
550 identify mutations predicted to lead to loss of function of *gdf6b*. Following identification
551 of candidate zebrafish by sequencing, zebrafish were bred to generate homozygous
552 *gdf6b(lf)* mutations. Whole RNA was isolated from homozygous *gdf6b(lf)* embryos at 20
553 HPF and qPCR was used to determine effective depletion of *gdf6b* transcripts. Primers
554 for genotyping and qPCR are listed in the Key Reagents section.

555

556 Construction of *Tg(mitfa:gdf6a)*

557 To generate the *Tg(mitfa:gdf6a)* transgenic line, 25 pg of pDestTol2CG2-mitfa:gdf6a:pA
558 was injected along with 25 pg of Tol2 transposase RNA, synthesized from pCS2FA-
559 transposase, into single cell wild-type embryos (Kwan et al., 2007). Embryos were
560 screened for incorporation of the transgene by expression of cmlc:eGFP in the heart at
561 48 HPF. Animals with eGFP-positive hearts (F0) were outcrossed to wild-type animals
562 to determine germline incorporation.

563

564 Drug Treatments

565 Drugs used in experiments were reconstituted at stock concentrations in solvent as
566 follows: DMH1 (BMPi), 10mM in DMSO; Tamoxifen (4-OHT), 1mg/mL in ethanol;
567 Epinephrine, 10mg/mL in embryo media. Embryos were dechorionated by incubating in
568 Pronase (Roche) for 10 minutes with gentle shaking. Dechorionated embryos were
569 transferred to 6-well plates coated in 1.5% agarose in embryo media. Embryo media
570 with appropriate drug concentration or vehicle control was added to each well. For BMPi
571 and 4-OHT treatments, embryos were treated from 12 HPF (6ss) to 24 HPF (Prim-5).
572 Embryos were incubated at 28.5°C for the duration of the drug treatment. Following
573 drug treatment, embryos were thoroughly washed in fresh embryo medium and returned
574 to incubator in new embryo medium until analysis.

575

576 Lineage Tracing

577 To trace the lineage of embryonic pigment cells, *Tg(ubi:switch)* embryos were injected
578 with 25 pg of pDestTol2pA2-mitfa:Cre-ERT2:pA and 25 pg of Tol2 transposase RNA at
579 the single-cell stage. At 12 HPF, injected embryos were treated with BMPi and 4-OHT

580 as described above. Following treatment, embryos were thoroughly washed and
581 allowed to mature at 28.5°C to 5 DPF. Embryos were treated with 1 mg/mL epinephrine
582 to contract melanosomes, anesthetized using 0.17mg/mL tricaine in embryo media,
583 mounted in 1% low-melt agarose on a plastic dish, and submerged in embryo media for
584 imaging.

585

586 Mosaic Rescue

587 MiniCoopR constructs MCR-mitfa:dnBMPR:pA, MCR-mitfa:SMAD1-DVD:pA, and MCR-
588 mitfa:eGFP:pA (control) were used. *mitfa(lf)* animals were injected with 25 pg of a single
589 construct and 25 pg of Tol2 transposase RNA. Upon successful integration of the MCR
590 constructs, the *mitfa*-minigene in the construct allowed development of melanocytes.
591 Embryos were screened for incorporation of the transgene by rescue of melanocytes at
592 5 DPF (Ceol et al., 2011).

593

594 In Situ Hybridization

595 RNA sense and anti-sense probes were synthesized from pcsDest2-*gdf6a* and
596 pcsDest2-*gdf6b* constructs using DIG RNA Labeling Kit (Roche) per the manufacturer's
597 instruction. Wild-type embryos of the appropriate stage were fixed in 4% PFA at 4°C for
598 24 hours. Following fixation, embryos were dehydrated in methanol and stored at -20°C.
599 Whole mount *in situ* hybridization was performed as previously described (Reichert et
600 al., 2013). Hybridized probes were detected using anti-digoxigenin (DIG) antibodies
601 tagged with alkaline-phosphatase (AP) (Roche) using NBT/BCIP (Roche) solution per
602 the manufacturer's instructions. Stained embryos were mounted in 2.5%

603 methylcellulose and imaged using a Leica M165FC microscope and Leica DFC400
604 camera. Specificity of the probes was verified using sense probes synthesized from the
605 same construct.

606

607 Immunofluorescence

608 Embryos were fixed at the desired time or following drug treatment in 4% PFA for 24
609 hours at 4°C. Whole mount immunofluorescence was performed as previously
610 described (Venkatesan et al., 2018). Primary antibodies used were pSMAD-1/5/8 (1:100
611 dilution) (Cell Signal Technologies), HuC/D (1:100 dilution) (Sigma), mitfa (1:100
612 dilution) (Venkatesan et al., 2018). AlexaFluor-488 (Invitrogen) and AlexaFluor-555
613 (Invitrogen) conjugated secondary antibodies were used to detect primary antibody
614 signaling. Nuclei were counterstained with DAPI. Following staining, animals were
615 dissected to remove yolk sack and flat mounted laterally on slides using VectaShield
616 mounting medium. Fluorescent images were taken using a Leica DM5500 microscope
617 with a Leica DFC365FX camera, and a Zeiss Axiovert 200 microscope outfitted with a
618 Yokogawa spinning disk confocal scanner. Cells and structures were counted, and data
619 was analyzed using Microsoft Excel and GraphPad Prism 7.

620

621 Flow Cytometry & Fluorescence Activated Cell Sorting (FACS)

622 Embryos were treated and matured to appropriate age as per drug treatment protocol
623 described above. At a desired timepoint, embryos were washed in PBS and transferred
624 to 500 µL of PBS + 5% FBS (FACS buffer). Embryos were mechanically dissociated in
625 FACS buffer using a mortar and pestle. Dissociated embryos were washed with FACS

626 buffer and filtered through a 40 μ m mesh membrane. Samples were analyzed using a
627 BD FACS Aria II flow cytometer and sorted directly into Trizol LS (Life Technologies) for
628 RNA isolation. Flow cytometry data was analyzed using FlowJo software (Becton,
629 Dickinson & Company) and GraphPad Prism 7.

630

631 Quantitative Real-Time PCR (qPCR)

632 Oligos used for qPCR primers are listed in Key Reagents section. RNA was isolated
633 from FACS-sorted cells or whole embryos using Trizol reagent (Life Technologies) and
634 purified using the RNeasy kit (Qiagen) per manufacturer's protocol. cDNA was
635 synthesized from purified RNA using the SuperScript III First Strand Synthesis kit
636 (Thermo Fisher). Reaction mixes were assembled with SYBR Green RT-PCR master
637 mix (Thermo Fisher), primers, and 25 ng cDNA, and analyzed using a StepOnePlus
638 Real Time PCR System (Applied Biosystems). Fold changes were calculated using the
639 $\Delta\Delta Ct$ method using Microsoft Excel and GraphPad Prism 7.

640

641 Imaging and Quantification

642 Zebrafish adults and embryos were treated with 1 mg/mL epinephrine to contract
643 melanosomes prior to imaging unless otherwise noted. Fish were anesthetized in 0.17%
644 Tricaine in embryo media and positioned in 2.5% methylcellulose in embryo media for
645 imaging. Images of adult fish were captured with a Nikon D90 DSLR camera. Brightfield
646 and incident light images of embryos were captured with Leica M165FC microscope
647 and Leica DFC400 camera. Fluorescent images of embryos were captured with a Leica
648 DM5500 upright microscope with a Leica DFC365FX camera, and a Zeiss Axiovert 200

649 microscope outfitted with a Yokogawa spinning disk confocal scanner. Images were
650 processed using ImageJ and Leica LAS X software. Cells were counted and analyses
651 were performed using Microsoft Excel and GraphPad Prism 7. Statistical calculations
652 were performed using GraphPad Prism 7 as described in each Figure legend.

653

654 **Statistical Analysis**

655 Statistical analyses were performing using GraphPad Prism 7 software package.
656 Statistical significance of experiments was calculated using Student's t-test, ratio-paired
657 t-test, Fisher's exact test with Bonferroni's correction, 1-way ANOVA with Tukey's
658 multiple comparison test as described in each figure legend. Statistical significance was
659 denoted as follows: not significant (ns) $P > 0.05$, $^*P<0.05$, $^{**}P<0.01$, $^{***}P<0.001$ and
660 $^{****}P<0.0001$.

661

662 **References**

663

664 Bruneau, S., & Rosa, F. M. (1997). Dynamo, a new zebrafish DVR member of the TGF-
665 β superfamily is expressed in the posterior neural tube and is up-regulated by
666 Sonic hedgehog. *Mechanisms of Development*, 61(1-2), 199-212.
667 doi:10.1016/s0925-4773(96)00641-7

668 Caramel, J., Papadogeorgakis, E., Hill, L., Browne, G. J., Richard, G., Wierinckx, A., . . .
669 Tulchinsky, E. (2013). A switch in the expression of embryonic EMT-inducers
670 drives the development of malignant melanoma. *Cancer Cell*, 24(4), 466-480.
671 doi:10.1016/j.ccr.2013.08.018

672 Carreira, S., Goodall, J., Denat, L., Rodriguez, M., Nuciforo, P., Hoek, K. S., . . . Goding,
673 C. R. (2006). Mitf regulation of Dia1 controls melanoma proliferation and
674 invasiveness. *Genes Dev*, 20(24), 3426-3439. doi:10.1101/gad.406406

675 Casas, E., Kim, J., Bendesky, A., Ohno-Machado, L., Wolfe, C. J., & Yang, J. (2011).
676 Snail2 is an essential mediator of Twist1-induced epithelial mesenchymal
677 transition and metastasis. *Cancer Res*, 71(1), 245-254. doi:10.1158/0008-
678 5472.CAN-10-2330

679 Cechmanek, P. B., & McFarlane, S. (2017). Retinal pigment epithelium expansion
680 around the neural retina occurs in two separate phases with distinct
681 mechanisms. *Dev Dyn*, 246(8), 598-609. doi:10.1002/dvdy.24525

682 Ceol, C. J., Houvras, Y., Jane-Valbuena, J., Bilodeau, S., Orlando, D. A., Battisti, V., . . .
683 Zon, L. I. (2011). The histone methyltransferase SETDB1 is recurrently amplified
684 in melanoma and accelerates its onset. *Nature*, 471(7339), 513-517.
685 doi:10.1038/nature09806

686 Chaffer, C. L., Brueckmann, I., Scheel, C., Kaestli, A. J., Wiggins, P. A., Rodrigues, L.
687 O., . . . Weinberg, R. A. (2011). Normal and neoplastic nonstem cells can
688 spontaneously convert to a stem-like state. *Proc Natl Acad Sci U S A*, 108(19),
689 7950-7955. doi:10.1073/pnas.1102454108

690 Curran, K., Lister, J. A., Kunkel, G. R., Prendergast, A., Parichy, D. M., & Raible, D. W.
691 (2010). Interplay between Foxd3 and Mitf regulates cell fate plasticity in the
692 zebrafish neural crest. *Dev Biol*, 344(1), 107-118.
693 doi:10.1016/j.ydbio.2010.04.023

694 Curran, K., Raible, D. W., & Lister, J. A. (2009). Foxd3 controls melanophore
695 specification in the zebrafish neural crest by regulation of Mitf. *Dev Biol*, 332(2),
696 408-417. doi:10.1016/j.ydbio.2009.06.010

697 Dougherty, M., Kamel, G., Grimaldi, M., Gfrerer, L., Shubinets, V., Ethier, R., . . . Liao,
698 E. C. (2013). Distinct requirements for wnt9a and irf6 in extension and integration
699 mechanisms during zebrafish palate morphogenesis. 140(1), 76-81.
700 doi:10.1242/dev.080473

701 Dravis, C., Chung, C. Y., Lytle, N. K., Herrera-Valdez, J., Luna, G., Trejo, C. L., . . .
702 Wahl, G. M. (2018). Epigenetic and Transcriptomic Profiling of Mammary Gland
703 Development and Tumor Models Disclose Regulators of Cell State Plasticity.
704 *Cancer Cell*, 34(3), 466-482 e466. doi:10.1016/j.ccr.2018.08.001

705 Dutton, K. A., Pauliny, A., Lopes, S. S., Elworthy, S., Carney, T. J., Rauch, J., . . . Kelsh,
706 R. N. (2001). Zebrafish *colourless* encodes *sox10* and
707 specifies non-ectomesenchymal neural crest fates. *Development*, 128(21), 4113-
708 4125. Retrieved from
709 <https://dev.biologists.org/content/develop/128/21/4113.full.pdf>

710 Elworthy, S., Lister, J. A., Carney, T. J., Raible, D. W., & Kelsh, R. N. (2003).
711 Transcriptional regulation of *mitfa* accounts for the *sox10* requirement in
712 zebrafish melanophore development. *Development*, 130(12), 2809-2818.
713 doi:10.1242/dev.00461

714 Eom, D. S., & Parichy, D. M. (2017). A macrophage relay for long-distance signaling
715 during postembryonic tissue remodeling. *Science*, 355(6331), 1317-1320.
716 doi:10.1126/science.aal2745

717 Fadeev, A., Krauss, J., Singh, A. P., & Nusslein-Volhard, C. (2016). Zebrafish
718 Leucocyte tyrosine kinase controls iridophore establishment, proliferation and
719 survival. *Pigment Cell Melanoma Res*, 29(3), 284-296. doi:10.1111/pcmr.12454

720 Fallahi-Sichani, M., Becker, V., Izar, B., Baker, G. J., Lin, J. R., Boswell, S. A., . . .
721 Sorger, P. K. (2017). Adaptive resistance of melanoma cells to RAF inhibition via
722 reversible induction of a slowly dividing de-differentiated state. *Mol Syst Biol*,
723 13(1), 905. doi:10.15252/msb.20166796

724 French, C. R., Erickson, T., French, D. V., Pilgrim, D. B., & Waskiewicz, A. J. (2009).
725 *Gdf6a* is required for the initiation of dorsal-ventral retinal patterning and lens
726 development. 333(1), 37-47. doi:10.1016/j.ydbio.2009.06.018

727 Garnett, A. T., Square, T. A., & Medeiros, D. M. (2012). BMP, Wnt and FGF signals are
728 integrated through evolutionarily conserved enhancers to achieve robust
729 expression of Pax3 and Zic genes at the zebrafish neural plate border.
730 *Development*, 139(22), 4220-4231. doi:10.1242/dev.081497

731 Gianino, S., Grider, J. R., Cresswell, J., Enomoto, H., & Heuckerth, R. O. (2003).
732 GDNF availability determines enteric neuron number by controlling precursor
733 proliferation. *Development*, 130(10), 2187-2198. doi:10.1242/dev.00433

734 Gosse, N. J., & Baier, H. (2009). An essential role for Radar (Gdf6a) in inducing dorsal
735 fate in the zebrafish retina. *Proc Natl Acad Sci U S A*, 106(7), 2236-2241.
736 doi:10.1073/pnas.0803202106

737 Gupta, P. B., Kuperwasser, C., Brunet, J. P., Ramaswamy, S., Kuo, W. L., Gray, J. W., . . .
738 Weinberg, R. A. (2005). The melanocyte differentiation program predisposes
739 to metastasis after neoplastic transformation. *Nat Genet*, 37(10), 1047-1054.
740 doi:10.1038/ng1634

741 Hanel, M. L., & Hensey, C. (2006). Eye and neural defects associated with loss of
742 GDF6. *BMC Developmental Biology*, 6(1), 43. doi:10.1186/1471-213x-6-43

743 Hao, J., Ho, J. N., Lewis, J. A., Karim, K. A., Daniels, R. N., Gentry, P. R., . . . Hong, C.
744 C. (2010). In vivo structure-activity relationship study of dorsomorphin analogues
745 identifies selective VEGF and BMP inhibitors. *ACS Chem Biol*, 5(2), 245-253.
746 doi:10.1021/cb9002865

747 Hashiguchi, M., & Mullins, M. C. (2013). Anteroposterior and dorsoventral patterning are
748 coordinated by an identical patterning clock. *Development*, 140(9), 1970-1980.
749 doi:10.1242/dev.088104

750 Hayano, S., Komatsu, Y., Pan, H., & Mishina, Y. (2015). Augmented BMP signaling in
751 the neural crest inhibits nasal cartilage morphogenesis by inducing p53-mediated
752 apoptosis. *Development*, 142(7), 1357-1367. doi:10.1242/dev.118802

753 Hoek, K. S., & Goding, C. R. (2010). Cancer stem cells versus phenotype-switching in
754 melanoma. *Pigment Cell Melanoma Res*, 23(6), 746-759. doi:10.1111/j.1755-
755 148X.2010.00757.x

756 Hoek, K. S., Schlegel, N. C., Brafford, P., Sucker, A., Ugurel, S., Kumar, R., . . .
757 Dummer, R. (2006). Metastatic potential of melanomas defined by specific gene
758 expression profiles with no BRAF signature. *Pigment Cell Res*, 19(4), 290-302.
759 doi:10.1111/j.1600-0749.2006.00322.x

760 Ignatius, M. S., Moose, H. E., El-Hodiri, H. M., & Henion, P. D. (2008). colgate/hdac1
761 Repression of foxd3 expression is required to permit mitfa-dependent
762 melanogenesis. *Dev Biol*, 313(2), 568-583. doi:10.1016/j.ydbio.2007.10.045

763 Jin, E. J., Erickson, C. A., Takada, S., & Burrus, L. W. (2001). Wnt and BMP signaling
764 govern lineage segregation of melanocytes in the avian embryo. *Dev Biol*,
765 233(1), 22-37. doi:10.1006/dbio.2001.0222

766 Kaufman, C. K., Mosimann, C., Fan, Z. P., Yang, S., Thomas, A. J., Ablain, J., . . . Zon,
767 L. I. (2016). A zebrafish melanoma model reveals emergence of neural crest
768 identity during melanoma initiation. *Science*, 351(6272), aad2197.
769 doi:10.1126/science.aad2197

770 Kishigami, S., & Mishina, Y. (2005). BMP signaling and early embryonic patterning.
771 *Cytokine Growth Factor Rev*, 16(3), 265-278. doi:10.1016/j.cytofr.2005.04.002

772 Knappe, N., Novak, D., Wein, K., Bernhardt, M., Reith, M., Larribere, L., . . . Utikal, J.
773 (2016). Directed Dedifferentiation Using Partial Reprogramming Induces Invasive
774 Phenotype in Melanoma Cells. *STEM CELLS*, 34(4), 832-846.
775 doi:10.1002/stem.2284

776 Kwan, K. M., Fujimoto, E., Grabher, C., Mangum, B. D., Hardy, M. E., Campbell, D. S., .
777 . Chien, C. B. (2007). The Tol2kit: a multisite gateway-based construction kit for
778 Tol2 transposon transgenesis constructs. *Dev Dyn*, 236(11), 3088-3099.
779 doi:10.1002/dvdy.21343

780 Landsberg, J., Kohlmeyer, J., Renn, M., Bald, T., Rogava, M., Cron, M., . . . Tuting, T.
781 (2012). Melanomas resist T-cell therapy through inflammation-induced reversible
782 dedifferentiation. *Nature*, 490(7420), 412-416. doi:10.1038/nature11538

783 Lewis, J. L., Bonner, J., Modrell, M., Ragland, J. W., Moon, R. T., Dorsky, R. I., &
784 Raible, D. W. (2004). Reiterated Wnt signaling during zebrafish neural crest
785 development. *Development*, 131(6), 1299-1308. doi:10.1242/dev.01007

786 Lister, J. A., Cooper, C., Nguyen, K., Modrell, M., Grant, K., & Raible, D. W. (2006).
787 Zebrafish Foxd3 is required for development of a subset of neural crest
788 derivatives. *Dev Biol*, 290(1), 92-104. doi:10.1016/j.ydbio.2005.11.014

789 Lister, J. A., Robertson, C. P., Lepage, T., Johnson, S. L., & Raible, D. W. (1999). nacre
790 encodes a zebrafish microphthalmia-related protein that regulates neural-crest-
791 derived pigment cell fate. *Development*, 126(17), 3757. Retrieved from
792 <http://dev.biologists.org/content/126/17/3757.abstract>

793 Liu, J., Fukunaga-Kalabis, M., Li, L., & Herlyn, M. (2014). Developmental pathways
794 activated in melanocytes and melanoma. *Arch Biochem Biophys*, 563, 13-21.
795 doi:10.1016/j.abb.2014.07.023

796 Lopes, S. S., Yang, X., Muller, J., Carney, T. J., McAdow, A. R., Rauch, G. J., . . .
797 Kelsh, R. N. (2008). Leukocyte tyrosine kinase functions in pigment cell
798 development. *PLoS Genet*, 4(3), e1000026. doi:10.1371/journal.pgen.1000026

799 McConnell, A. M., Mito, J. K., Ablain, J., Dang, M., Formichella, L., Fisher, D. E., & Zon,
800 L. I. (2019). Neural crest state activation in NRAS driven melanoma, but not in
801 NRAS-driven melanocyte expansion. *Dev Biol*, 449(2), 107-114.
802 doi:10.1016/j.ydbio.2018.05.026

803 McGraw, H. F., Nechiporuk, A., & Raible, D. W. (2008). Zebrafish dorsal root ganglia
804 neural precursor cells adopt a glial fate in the absence of neurogenin1. *J
805 Neurosci*, 28(47), 12558-12569. doi:10.1523/JNEUROSCI.2079-08.2008

806 McMahon, J. A., Takada, S., Zimmerman, L. B., Fan, C. M., Harland, R. M., &
807 McMahon, A. P. (1998). Noggin-mediated antagonism of BMP signaling is
808 required for growth and patterning of the neural tube and somite. *Genes Dev*,
809 12(10), 1438-1452. doi:10.1101/gad.12.10.1438

810 Mehta, A., Kim, Y. J., Robert, L., Tsoi, J., Comin-Anduix, B., Berent-Maoz, B., . . .
811 Ribas, A. (2018). Immunotherapy Resistance by Inflammation-Induced
812 Dedifferentiation. *Cancer Discov*, 8(8), 935-943. doi:10.1158/2159-8290.CD-17-
813 1178

814 Mosimann, C., Kaufman, C. K., Li, P., Pugach, E. K., Tamplin, O. J., & Zon, L. I. (2011).
815 Ubiquitous transgene expression and Cre-based recombination driven by the
816 ubiquitin promoter in zebrafish. *Development*, 138(1), 169-177.
817 doi:10.1242/dev.059345

818 Muller, J., Krijgsman, O., Tsoi, J., Robert, L., Hugo, W., Song, C., . . . Peeper, D. S.
819 (2014). Low MITF/AXL ratio predicts early resistance to multiple targeted drugs in
820 melanoma. *Nat Commun*, 5, 5712. doi:10.1038/ncomms6712

821 Nagao, Y., Takada, H., Miyadai, M., Adachi, T., Seki, R., Kamei, Y., . . . Hashimoto, H.
822 (2018). Distinct interactions of Sox5 and Sox10 in fate specification of pigment
823 cells in medaka and zebrafish. *PLoS Genet*, 14(4), e1007260.
824 doi:10.1371/journal.pgen.1007260

825 Nikaido, M., Tada, M., Saji, T., & Ueno, N. (1997). Conservation of BMP signaling in
826 zebrafish mesoderm patterning. *Mech Dev*, 61(1-2), 75-88.
827 doi:[https://doi.org/10.1016/S0925-4773\(96\)00625-9](https://doi.org/10.1016/S0925-4773(96)00625-9)

828 Nojima, J., Kanomata, K., Takada, Y., Fukuda, T., Kokabu, S., Ohte, S., . . . Katagiri, T.
829 (2010). Dual roles of smad proteins in the conversion from myoblasts to
830 osteoblastic cells by bone morphogenetic proteins. *J Biol Chem*, 285(20), 15577-
831 15586. doi:10.1074/jbc.M109.028019

832 Nord, H., Dennhag, N., Muck, J., & von Hofsten, J. (2016). Pax7 is required for
833 establishment of the xanthophore lineage in zebrafish embryos. *Mol Biol Cell*,
834 27(11), 1853-1862. doi:10.1091/mbc.E15-12-0821

835 O'Brien-Ball, C., & Biddle, A. (2017). Reprogramming to developmental plasticity in
836 cancer stem cells. *Dev Biol*, 430(2), 266-274. doi:10.1016/j.ydbio.2017.07.025

837 Parichy, D. M., Ransom, D. G., Paw, B., Zon, L. I., & Johnson, S. L. (2000). An
838 orthologue of the kit-related gene fms is required for development of neural crest-
839 derived xanthophores and a subpopulation of adult melanocytes in the zebrafish,
840 *Danio rerio*. *Development*, 127(14), 3031-3044. Retrieved from
841 <https://dev.biologists.org/content/develop/127/14/3031.full.pdf>

842 Parichy, D. M., & Spiewak, J. E. (2015). Origins of adult pigmentation: diversity in
843 pigment stem cell lineages and implications for pattern evolution. *Pigment Cell
844 Melanoma Res*, 28(1), 31-50. doi:10.1111/pcmr.12332

845 Patterson, L. B., & Parichy, D. M. (2013). Interactions with iridophores and the tissue
846 environment required for patterning melanophores and xanthophores during
847 zebrafish adult pigment stripe formation. *PLoS Genet*, 9(5), e1003561.
848 doi:10.1371/journal.pgen.1003561

849 Perego, M., Maurer, M., Wang, J. X., Shaffer, S., Muller, A. C., Parapatics, K., . . .
850 Herlyn, M. (2018). A slow-cycling subpopulation of melanoma cells with highly
851 invasive properties. *Oncogene*, 37(3), 302-312. doi:10.1038/onc.2017.341

852 Petratou, K., Subkhankulova, T., Lister, J. A., Rocco, A., Schwetlick, H., & Kelsh, R. N.
853 (2018). A systems biology approach uncovers the core gene regulatory network
854 governing iridophore fate choice from the neural crest. *PLoS Genet*, 14(10),
855 e1007402. doi:10.1371/journal.pgen.1007402

856 Pyati, U. J., Webb, A. E., & Kimelman, D. (2005). Transgenic zebrafish reveal stage-
857 specific roles for Bmp signaling in ventral and posterior mesoderm development.
858 *Development*, 132(10), 2333-2343. doi:10.1242/dev.01806

859 Quigley, I. K., Turner, J. M., Nuckles, R. J., Manuel, J. L., Budi, E. H., MacDonald, E. L.,
860 & Parichy, D. M. (2004). Pigment pattern evolution by differential deployment of
861 neural crest and post-embryonic melanophore lineages in *Danio* fishes.
862 *Development*, 131(24), 6053-6069. doi:10.1242/dev.01526

863 Reed, N. P., & Mortlock, D. P. (2010). Identification of a distant cis-regulatory element
864 controlling pharyngeal arch-specific expression of zebrafish gdf6a/radar. *Dev*
865 *Dyn*, 239(4), 1047-1060. doi:10.1002/dvdy.22251

866 Reichert, S., Randall, R. A., & Hill, C. S. (2013). A BMP regulatory network controls
867 ectodermal cell fate decisions at the neural plate border. *Development*, 140(21),
868 4435-4444. doi:10.1242/dev.098707

869 Rissi, M., Wittbrodt, J., Délot, E., Naegeli, M., & Rosa, F. M. (1995). Zebrafish Radar: A
870 new member of the TGF- β superfamily defines dorsal regions of the neural plate
871 and the embryonic retina. 49(3), 223-234. doi:10.1016/0925-4773(94)00320-m

872 Rosai, J., & Ackerman, L. V. (1979). The pathology of tumors, part III: grading, staging
873 & classification. *CA Cancer J Clin*, 29(2), 66-77. doi:10.3322/canjclin.29.2.66

874 Sato, T. (2005). Neural crest determination by co-activation of Pax3 and Zic1 genes in
875 *Xenopus* ectoderm. 132(10), 2355-2363. doi:10.1242/dev.01823

876 Sauka-Spengler, T., Meulemans, D., Jones, M., & Bronner-Fraser, M. (2007). Ancient
877 evolutionary origin of the neural crest gene regulatory network. *Dev Cell*, 13(3),
878 405-420. doi:10.1016/j.devcel.2007.08.005

879 Schumacher, J. A., Hashiguchi, M., Nguyen, V. H., & Mullins, M. C. (2011). An
880 intermediate level of BMP signaling directly specifies cranial neural crest
881 progenitor cells in zebrafish. *PLoS One*, 6(11), e27403.
882 doi:10.1371/journal.pone.0027403

883 Shaffer, S. M., Dunagin, M. C., Torborg, S. R., Torre, E. A., Emert, B., Krepler, C., . . .
884 Raj, A. (2017). Rare cell variability and drug-induced reprogramming as a mode
885 of cancer drug resistance. *Nature*, 546(7658), 431-435. doi:10.1038/nature22794

886 Shakhova, O., Cheng, P., Mishra, P. J., Zingg, D., Schaefer, S. M., Debbache, J., . . .
887 Sommer, L. (2015). Antagonistic Cross-Regulation between Sox9 and Sox10
888 Controls an Anti-tumorigenic Program in Melanoma. 11(1), e1004877.
889 doi:10.1371/journal.pgen.1004877

890 Sidi, S., Goutel, C., Peyrieras, N., & Rosa, F. M. (2003). Maternal induction of ventral
891 fate by zebrafish radar. *Proc Natl Acad Sci U S A*, 100(6), 3315-3320.
892 doi:10.1073/pnas.0530115100

893 Southard-Smith, E. M., Kos, L., & Pavan, W. J. (1998). Sox10 mutation disrupts neural
894 crest development in Dom Hirschsprung mouse model. *Nat Genet*, 18(1), 60-64.
895 doi:10.1038/ng0198-60

896 Thomas, A. J., & Erickson, C. A. (2009). FOXD3 regulates the lineage switch between
897 neural crest-derived glial cells and pigment cells by repressing MITF through a
898 non-canonical mechanism. *Development*, 136(11), 1849-1858.
899 doi:10.1242/dev.031989

900 Tulchinsky, E., Pringle, J. H., Caramel, J., & Ansieau, S. (2014). Plasticity of melanoma
901 and EMT-TF reprogramming. *Oncotarget*, 5(1), 1-2.
902 doi:10.18632/oncotarget.1662

903 Valdivia, L. E., Lamb, D. B., Horner, W., Wierzbicki, C., Tafessu, A., Williams, A. M., . . .
904 Cerveny, K. L. (2016). Antagonism between Gdf6a and retinoic acid pathways
905 controls timing of retinal neurogenesis and growth of the eye in zebrafish.
906 *Development*, 143(7), 1087-1098. doi:10.1242/dev.130922

907 Venkatesan, A. M., Vyas, R., Gramann, A. K., Dresser, K., Gujja, S., Bhatnagar, S., . . .
908 Ceol, C. J. (2018). Ligand-activated BMP signaling inhibits cell differentiation and

909 death to promote melanoma. *J Clin Invest*, 128(1), 294-308.
910 doi:10.1172/JCI92513

911 Villefranc, J. A., Amigo, J., & Lawson, N. D. (2007). Gateway compatible vectors for
912 analysis of gene function in the zebrafish. *Dev Dyn*, 236(11), 3077-3087.
913 doi:10.1002/dvdy.21354

914 Westerfield, M. (1995). *The zebrafish book: a guide for the laboratory use of zebrafish*
915 (*Brachydanio rerio*): University of Oregon press.

916 Zuo, Q., Liu, J., Huang, L., Qin, Y., Hawley, T., Seo, C., . . . Yu, Y. (2018). AXL/AKT
917 axis mediated-resistance to BRAF inhibitor depends on PTEN status in
918 melanoma. *Oncogene*, 37(24), 3275-3289. doi:10.1038/s41388-018-0205-4

919

920

921

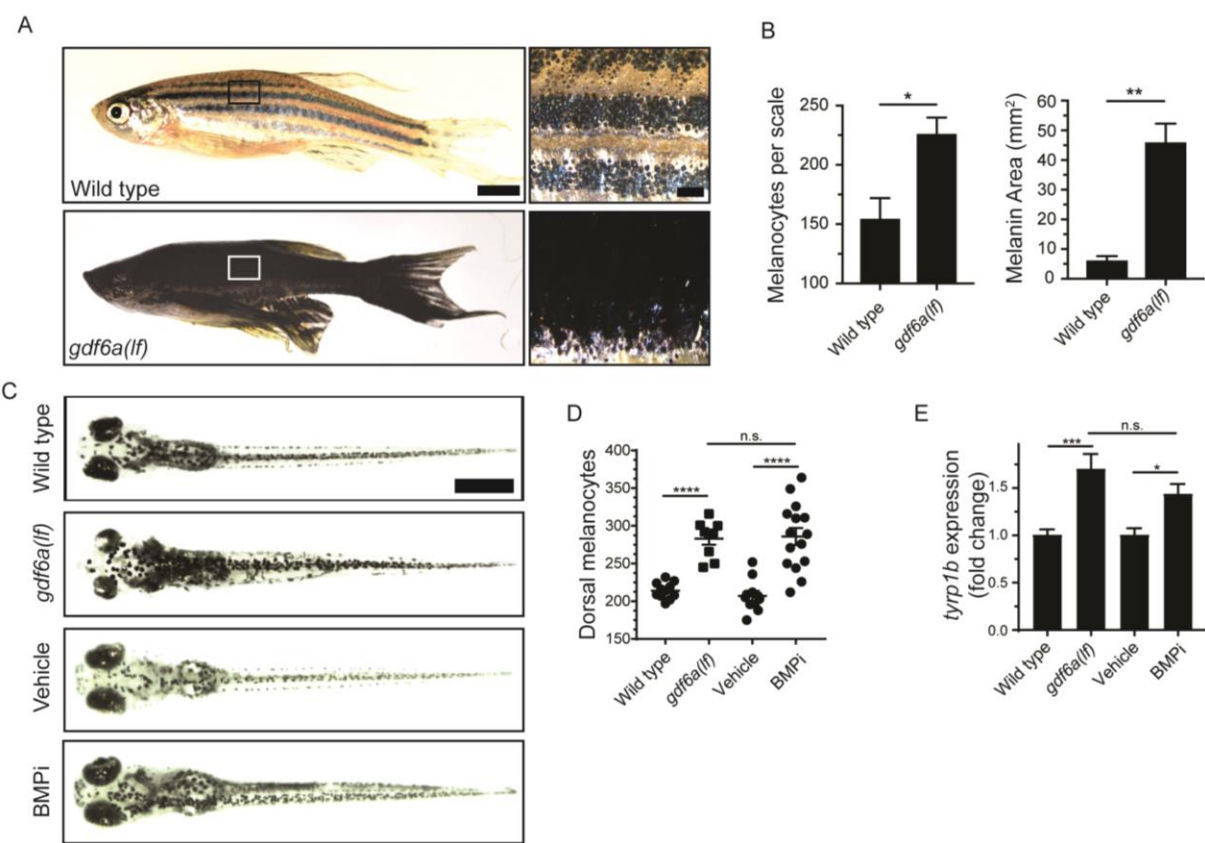
922

923

924

925

Figure 1



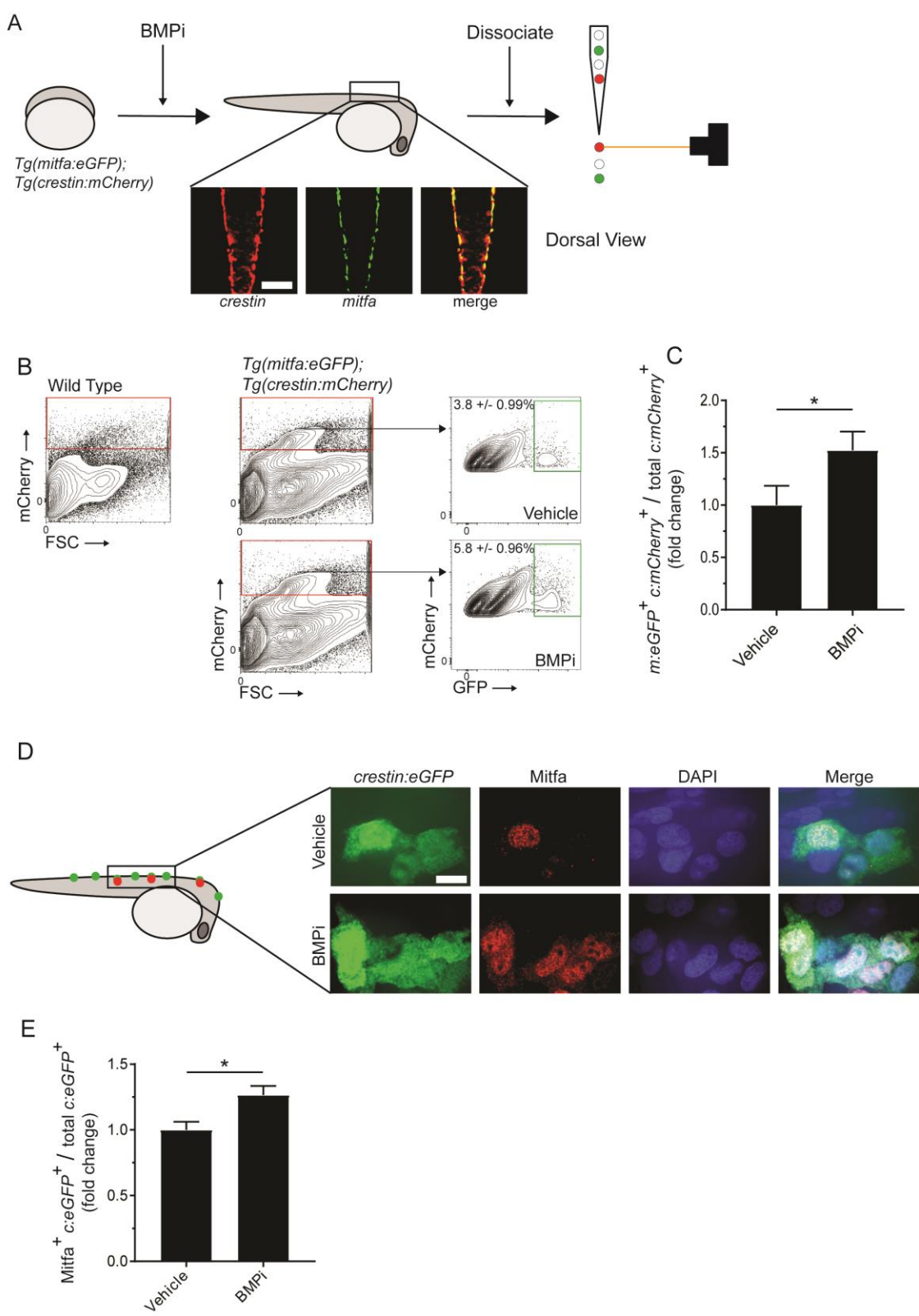
926

927

928 **Figure 1. *gdf6a* loss or BMP inhibition causes the development of supernumerary**
929 **melanocytes**

930 (A) Images of wild-type and *gdf6a(lf)* adult zebrafish, scale bar = 4 mm, inset scale bar
931 = 1 mm. (B) Quantification of number of melanocytes (left) and scale pigmentation using
932 melanin coverage (right), n = 3 scales per group. (C) Wild-type and *gdf6a(lf)* embryos
933 imaged at 5 days post fertilization (DPF); vehicle- and BMPi-treated embryos imaged at
934 5 DPF. Scale bar = 1 mm. Animals were treated with epinephrine prior to imaging. (D)
935 Quantification of dorsal melanocytes per animal in 5 DPF wild-type, *gdf6a(lf)* mutant,
936 vehicle-, and BMPi-treated embryos. n = 11, 9, 11, and 15, respectively. (E) Expression
937 of *tyrp1b* by qPCR in wild-type, *gdf6a(lf)* mutant, vehicle-, and BMPi-treated embryos. n
938 = 5-6 for each group. Error bars represent mean +/- SEM. P-values were calculated
939 using Student's t-test in panel B and one-way ANOVA with Tukey's multiple
940 comparisons test in panels D and E, * P<0.05, ** P<0.01, *** P<0.001, **** P<0.0001,
941 n.s., not significant.

Figure 2

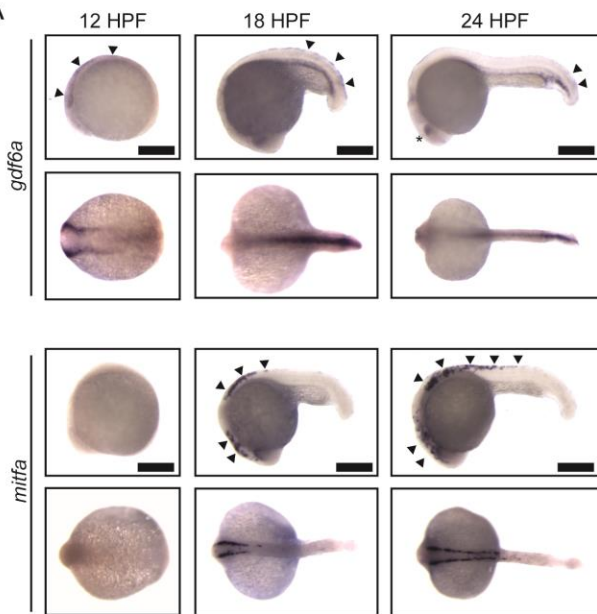


944 **Figure 2. Inhibition of BMP signaling increases *mitfa*-positive neural crest cells**

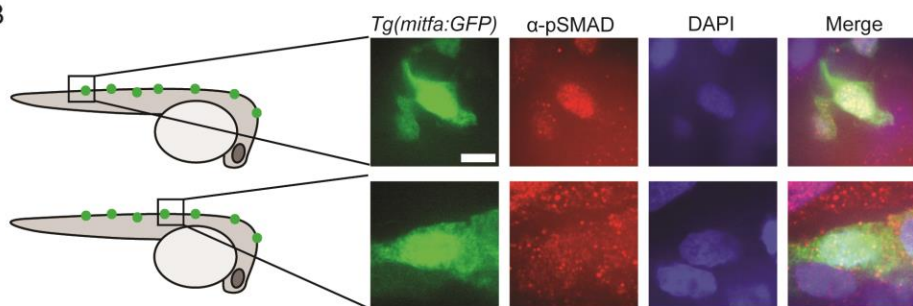
945 (A) Diagram of experiment. *Tg(crestin:mCherry); Tg(mitfa:eGFP)* embryos were treated
946 with BMPi from 12 to 24 HPF. At 24 HPF, embryos were dissociated and analyzed via
947 flow cytometry for GFP- and mCherry-positive cells, scale bar = 200 μ m. (B) Gating
948 strategy based on non-transgenic wild-type control to identify *crestin:mCherry*-positive
949 cells and *crestin:mCherry/mitfa:eGFP* double-positive cells. Top, control vehicle-treated
950 embryos. Bottom, BMPi-treated embryos. (C) Fold change in
951 *crestin:mCherry/mitfa:eGFP* double-positive cells per total *crestin:mCherry*-positive cells
952 in vehicle and BMPi-treated groups, n = 3 biological replicates of 80-100 stage-matched
953 embryos pooled for each condition. *m:eGFP*, *mitfa:eGFP*; *c:mCherry*, *crestin:mCherry*.
954 (D) anti-Mitfa immunofluorescence in *Tg(crestin:eGFP)* embryos treated with BMPi or
955 vehicle control and fixed at 24 hours, scaled bar = 10 μ m. (E) Fold change in
956 Mitfa/*crestin:eGFP* double-positive cells per total *crestin:eGFP*-cells, n = 16 embryos for
957 each condition. *c:eGFP*, *crestin:eGFP*. Error bars represent mean +/- SEM; P-value was
958 calculated using ratio-paired t-test in panel C and Student's t-test in panel E, * P < 0.05.

Figure 3

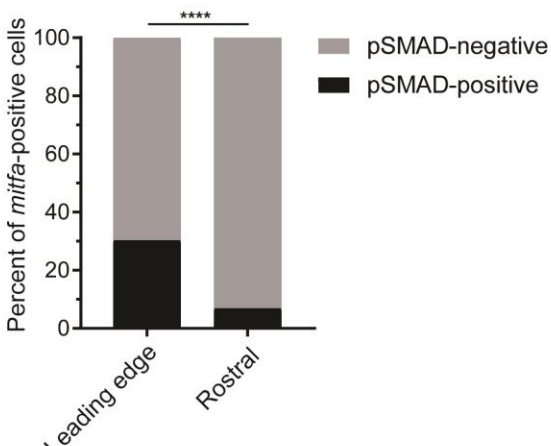
A



B



C



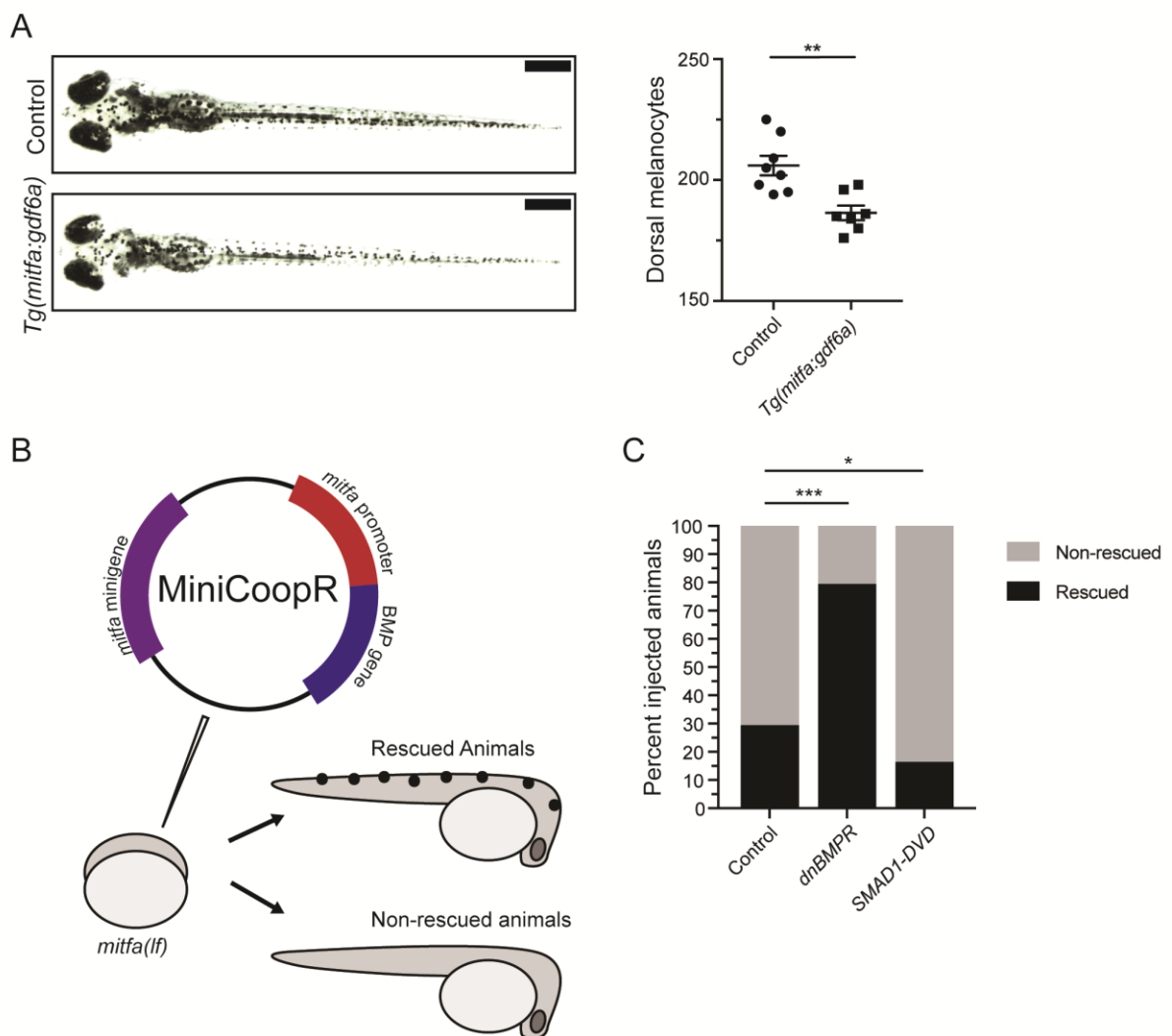
959

960

961 **Figure 3. *gdf6a* expression and BMP activity in pigment progenitor cells**

962 (A) RNA *in situ* hybridization for *gdf6a* (top) and *mitfa* (bottom) at 12-, 18-, and 24-hours
963 post-fertilization. Arrowheads indicate expression domains in the neural crest of *gdf6a*
964 and *mitfa*. Asterisk indicates known dorsal retinal expression of *gdf6a*. Scale bar = 500
965 μ m. (B) Images of GFP-positive cells from *Tg(mitfa:eGFP)* zebrafish stained with α -
966 pSMAD 1/5/8 antibody. Scale bar = 10 μ m. (C) Quantification of *mitfa:eGFP*-positive
967 cells that are phospho-SMAD1/5/8-positive. The leading edge encompassed 5 most
968 caudal *mitfa*-positive cells, whereas rostral cells included any *mitfa*-positive cells rostral
969 to the leading edge. n = 102 and 186 for distal leading edge and rostral cells,
970 respectively. P-value was calculated using Fisher's exact test, **** P < 0.0001.

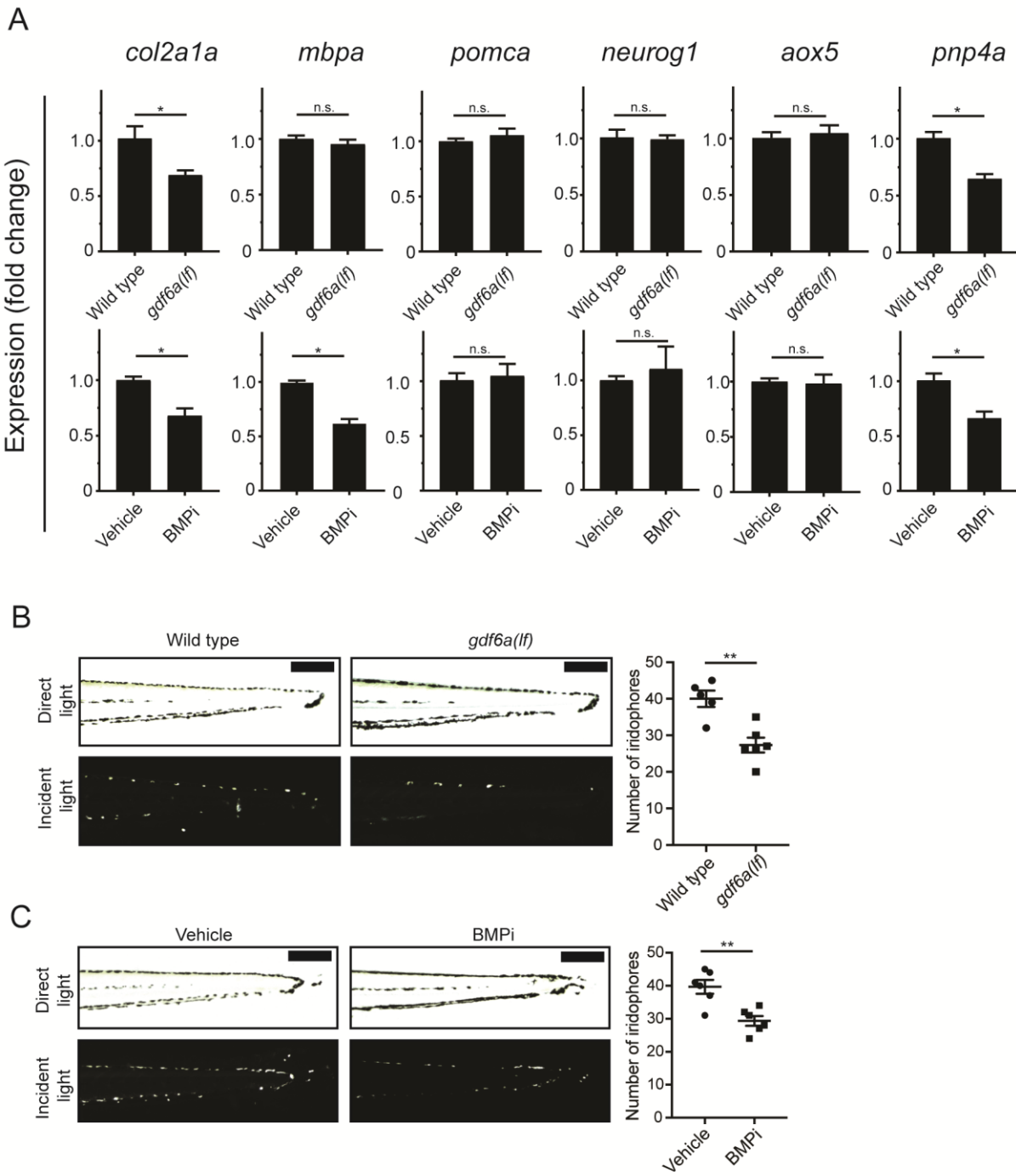
Figure 4



972 **Figure 4. BMP signaling within pigment progenitor cells can impact embryonic**
973 **melanocytes**

974 (A) *Tg(mitfa:gdf6a)* and non-transgenic sibling control embryos (left), and quantification
975 of dorsal melanocytes per animal in each group (right). Animals were treated with
976 epinephrine prior to imaging at 5 DPF, n = 8 and 7 for control and *Tg(mitfa:gdf6a)*
977 groups, respectively. Scale bar = 1 mm. (B) Diagram of miniCoopR rescue experiment.
978 Animals harboring a *mitfa(lf)* mutation were injected at the single-cell stage with the
979 miniCoopR vector containing a BMP gene. Animals were evaluated at 5 DPF for the
980 presence of melanocytes. If melanocytes were present, that animal was scored as
981 rescued, whereas animals lacking melanocytes were scored as non-rescued. (C)
982 Percentages of rescued and non-rescued animals following injection of a miniCoopR-
983 BMP vector, n = 361, 193 and 152 for control, *dnBMPR*, and *SMAD1-DVD* groups,
984 respectively. Error bars represent mean +/- SEM. P-values were calculated Student's t-
985 test for panel A and with Fisher's exact test with Bonferroni's correction for panel C, * P
986 <0.05, ** P <0.01, *** P <0.001.

Figure 5

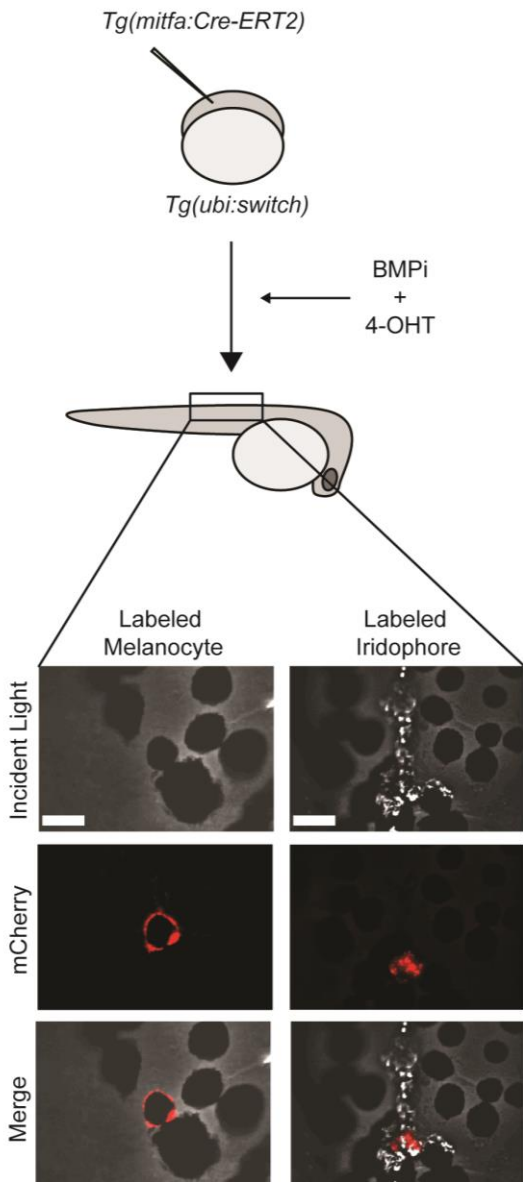


989 **Figure 5. *gdf6a* loss and BMP inhibition impact development of specific neural
990 crest derivatives**

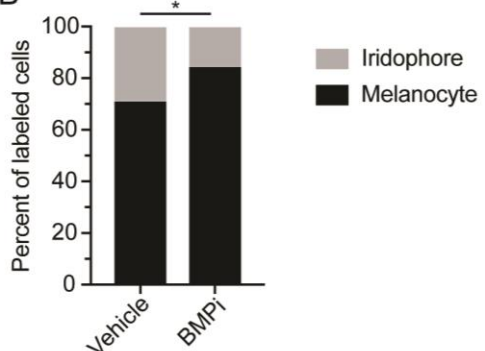
991 (A) Expression analyses of multiple neural crest lineage markers. qPCR was used to
992 assess changes in markers of neural crest derivatives in *gdf6a(lf)* embryonic zebrafish
993 (top) and BMPi-treated wild-type zebrafish (bottom) at 5 DPF; *col2a1a*, chondrocytes;
994 *mbpa*, glial; *pomca*, adrenal medullary cells; *neurog1*, neuronal cells; *aox5*,
995 xanthophores; *pnp4a*, iridophores; n = 5-6 for each group. (B) Direct light (top) and
996 incident light (bottom) images of wild-type and *gdf6a(lf)* embryos at 5 DPF and
997 quantification of dorsal iridophores (right) per animal in each group. Animals were
998 treated with epinephrine prior to imaging at 5 DPF; n = 5 and 6 for wild-type and
999 *gdf6a(lf)* groups, respectively; scale bar = 500 μ m. (C) Direct light, top, and incident
1000 light, bottom, images of wild-type embryos treated with vehicle or BMPi from 12 to 24
1001 HPF and quantification of dorsal iridophores, right, per animal in vehicle and BMPi
1002 treated groups. Animals treated with epinephrine prior to imaging at 5 DPF, n = 6 and 6
1003 for vehicle and BMPi groups, respectively; scale bar = 1 mm. Error bars represent mean
1004 +/- SEM, P-values calculated with Student's t-test, * P < 0.05, ** P < 0.01, n.s., not
1005 significant.

Figure 6

A



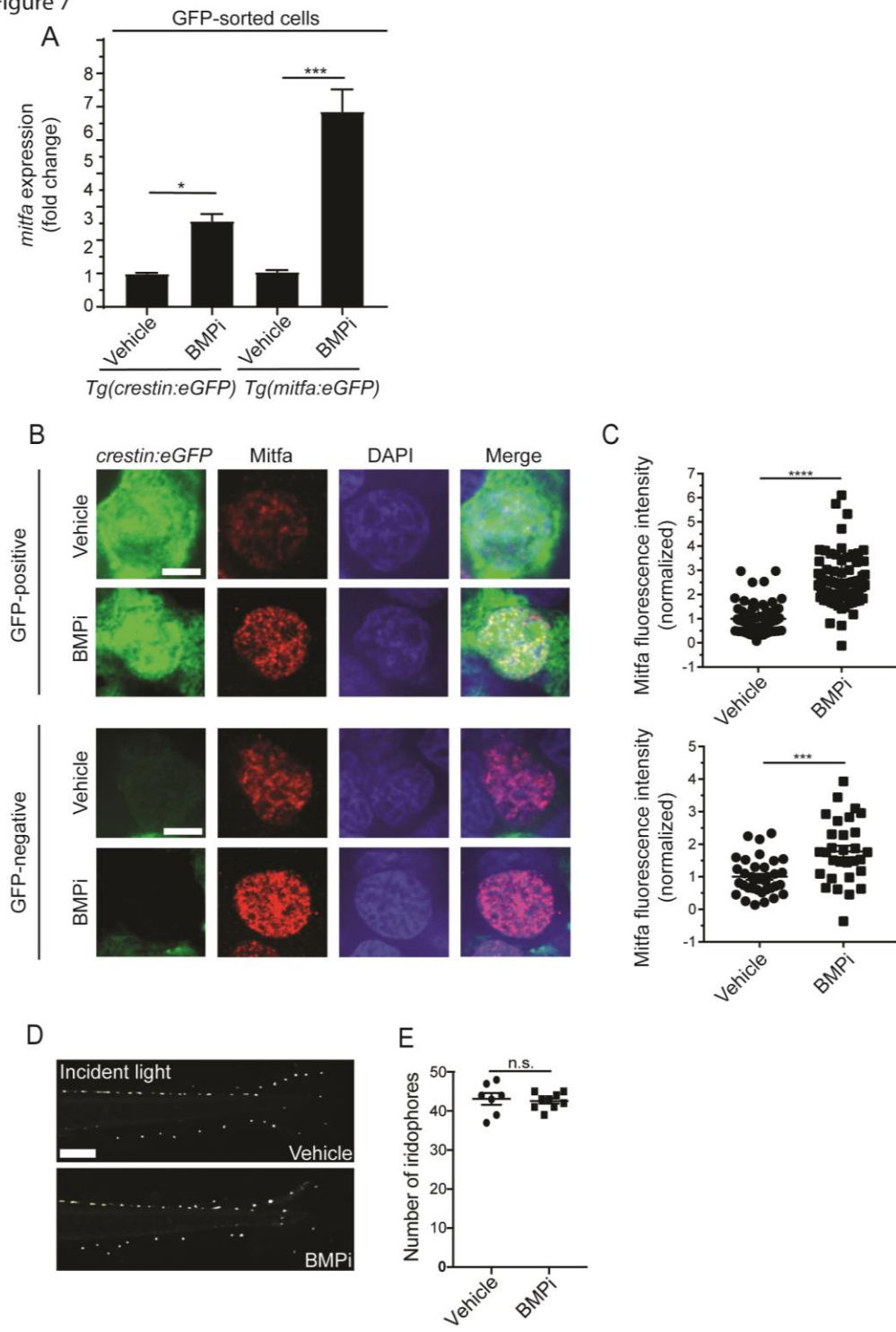
B



1007 **Figure 6. BMP inhibition impacts fate specification of *mitfa*-positive pigment**
1008 **progenitor cells**

1009 (A) Diagram of lineage tracing experiment. Embryos containing *Tg(ubi:switch)* were
1010 injected with a *mitfa:Cre-ERT2* construct and treated with BMPi and tamoxifen (4-OHT)
1011 from 12 to 24 HPF to block BMP signaling and allow Cre recombination. At 5 DPF,
1012 animals were screened for successful recombination by presence of single mCherry-
1013 labeled pigment cells, and the identities of those cells were assessed using incident
1014 light. Scale bar = 40 μ m. (B) Quantification of mCherry-labeled cell fates at 5 DPF in
1015 vehicle and BMPi-treated animals, n = 101 and 80 for vehicle and BMPi groups,
1016 respectively; P-value calculated using Fisher's exact test, * P < 0.05.

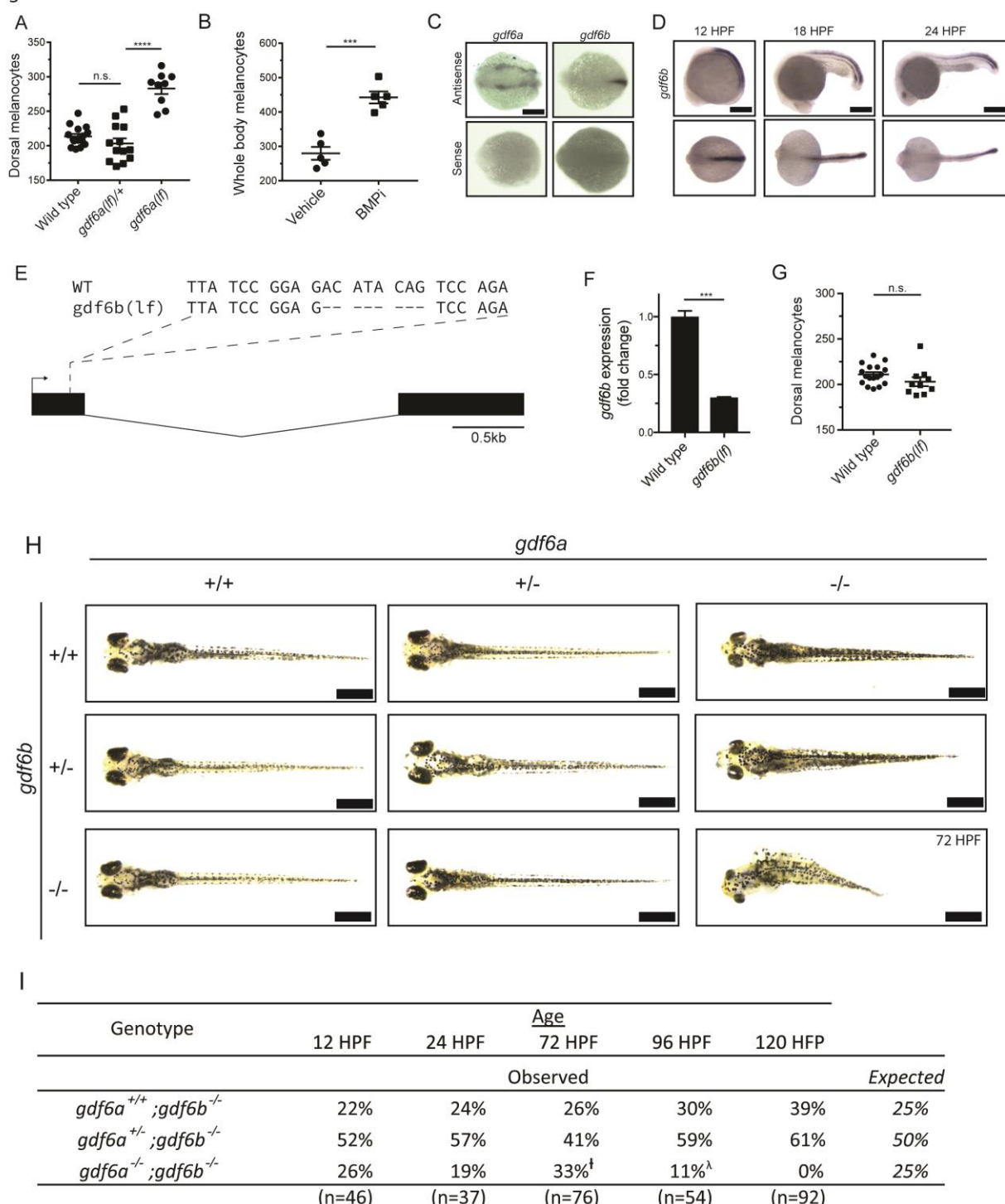
Figure 7



1018 **Figure 7. BMP signaling regulates expression of and acts through *mitfa* to impact**
1019 **pigment cell fates**

1020 (A) *mitfa* expression in sorted GFP-positive cells from *Tg(crestin:eGFP)* and
1021 *Tg(mitfa:eGFP)* embryos treated with vehicle or BMPi from 12 to 24 HPF, n = 4-5 for
1022 each condition. (B) anti-Mitfa immunofluorescence, DAPI and merged images of
1023 *Tg(crestin:eGFP)* embryos treated with vehicle control or BMPi in GFP-positive cells
1024 (top) and GFP-negative cells (bottom), scale bar = 5 μ m. (C) Quantification of anti-Mitfa
1025 fluorescence intensity of individual nuclei in GFP-positive cells (top) and GFP-negative
1026 cells (bottom); n = 65 and 74 for GFP-positive vehicle and BMPi groups, respectively; n
1027 = 35 and 30 for GFP-negative vehicle and BMPi groups, respectively. (D) Incident light
1028 images of *mitfa(lf)* embryonic zebrafish treated with vehicle or BMPi from 12 to 24 HPF
1029 and imaged at 5 DPF, scale bar = 1 mm. (E) Quantification of dorsal iridophores in
1030 *mitfa(lf)* embryonic zebrafish treated with vehicle or BMPi from 12 to 24 HPF, n = 7 and
1031 9 for vehicle and BMPi groups, respectively. Error bars represent mean +/- SEM, P-
1032 value was calculated using one-way ANOVA with Tukey's multiple comparisons test in
1033 panel A and Student's t-test in panel C and E. * P <0.05, *** P <0.001, **** P<0.0001,
1034 n.s., not significant.

Figure S1



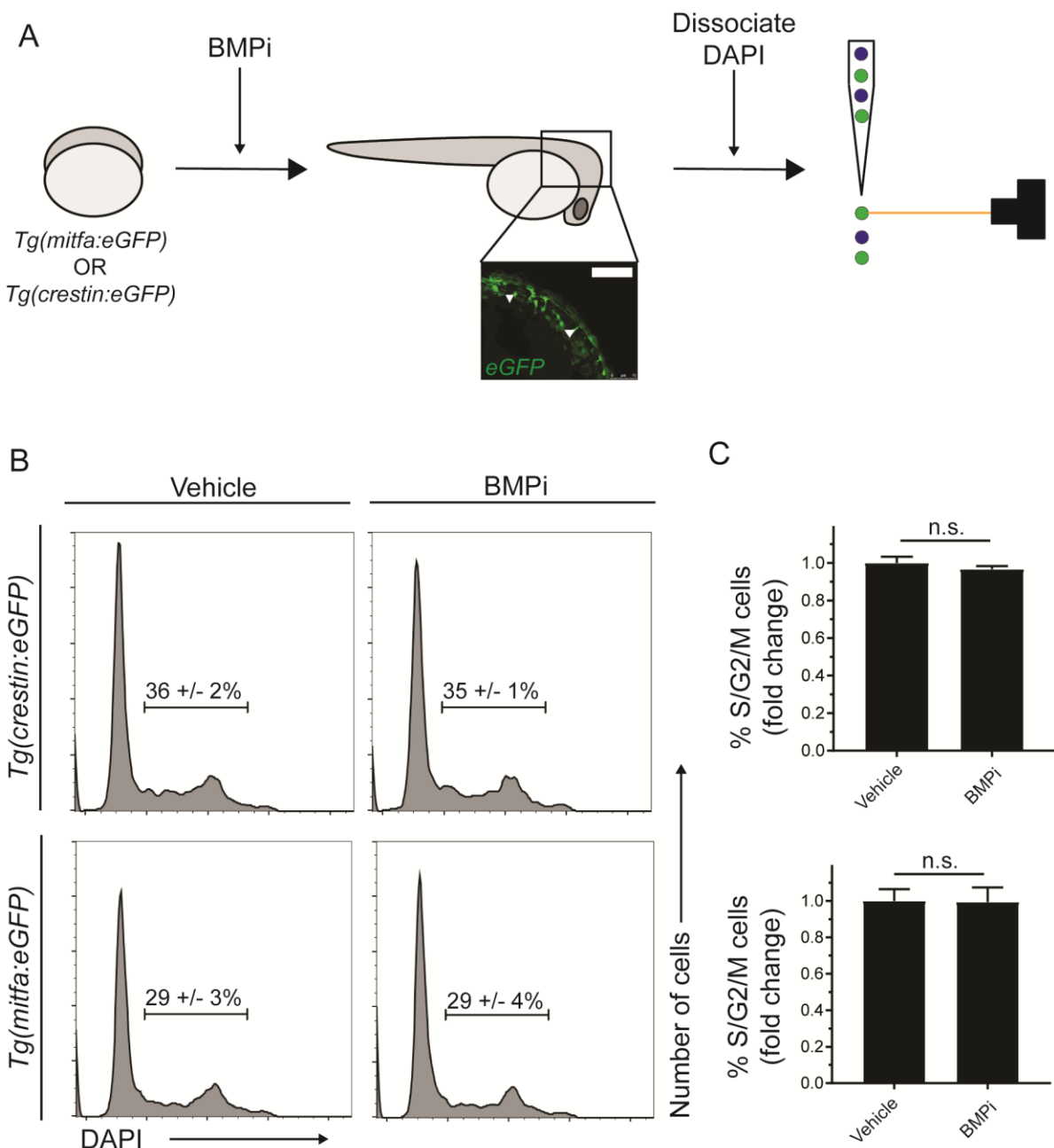
[†]Surviving embryos had various morphologic defects (cardiac edema, 64%; hydrocephalus, 20%; dysmorphic retina, 96%; body length deficit, 96%; dorsalization, 72%)

^λSurviving embryos had various morphologic defects (cardiac edema, 83%; hydrocephalus, 67%; dysmorphic retina, 100%; body length deficit, 100%; dorsalization, 100%)

1036 **Figure S1 (Related to Figure 1). *gdf6* paralogs are necessary for normal**
1037 **embryonic development**

1038 (A) Quantification of dorsal melanocytes in *gdf6a(lf/+)* heterozygotes, *gdf6a(lf)*
1039 homozygotes and wild-type embryos. (B) Quantification of whole-body melanocytes in
1040 vehicle- and BMPi-treated embryos. (C) Verification of *gdf6a* and *gdf6b* probe
1041 specificity. (D) RNA *in situ* hybridization for *gdf6b* at 12-, 18-, and 24-hours post-
1042 fertilization, scale bar = 500 μ m. (E) Sequence of *gdf6b(lf)* mutant indicating deletion
1043 and frameshift in exon 1. (F) Decreased *gdf6b* expression in *gdf6b(lf)* embryos. (G)
1044 Quantification of dorsal melanocytes in *gdf6b(lf)* mutants compared to wild-type
1045 embryos. (H) Images of *gdf6a(lf)* and *gdf6b(lf)* mutant combinations. *gdf6b(lf)* animals
1046 have no morphologic defects compared to wild-type embryos at 5 DPF, while *gdf6a(lf)*
1047 animals show pigmentation and eye morphology defects. *gdf6a(lf);gdf6b(lf)* double
1048 mutants show significant morphologic defects associated with *gdf6a(lf)* as well as
1049 decreased body length, cardiac edema and hydrocephalus. Scale bar = 1 mm. (I)
1050 Survival of *gdf6b(lf)* embryos with *gdf6a(lf)* mutations. \dagger , surviving embryos had various
1051 morphologic defects (cardiac edema, 64%; hydrocephalus, 20%; dysmorphic retina,
1052 96%; body length deficit, 96%; dorsalization, 72%). λ , surviving embryos had various
1053 morphologic defects (cardiac edema, 83%; hydrocephalus, 67%; dysmorphic retina,
1054 100%; body length deficit, 100%; dorsalization, 100%). Error bars represent mean +/-
1055 SEM. P-values were calculated using one-way ANOVA with Tukey's multiple
1056 comparison test for panel A and with Student's t-test for panels B, F, and G. *** P <
1057 0.001, **** P <0.0001, n.s., not significant.

Figure S2

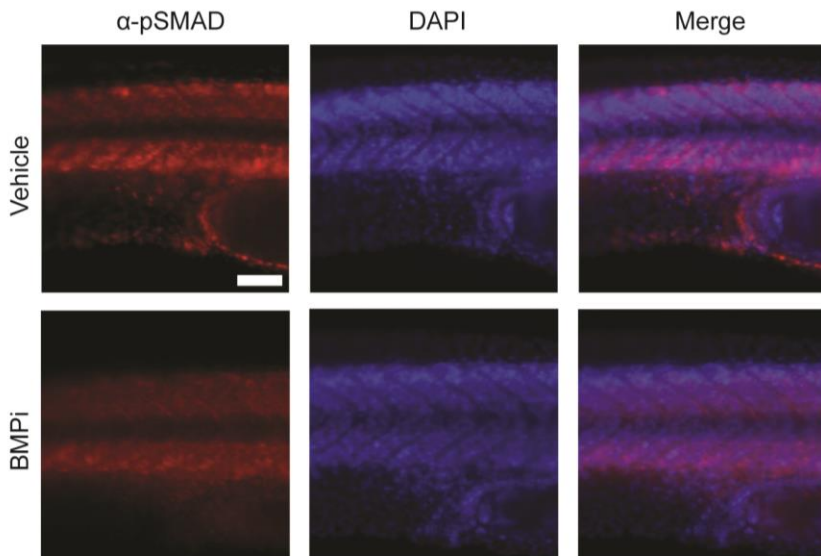


1058

1059 **Figure S2 (Related to Figure 2). Increased proliferation is not observed in neural
1060 crest and pigment progenitor cell populations of BMPi-treated embryos**

1061 (A) Diagram of experiment. Embryos expressing either *Tg(mitfa:eGFP)* or
1062 *Tg(crestin:eGFP)* were treated with BMP inhibitor from 12 to 24 HPF. Following
1063 treatment, embryos were dissociated, fixed, and stained for DNA content using DAPI
1064 and analyzed via flow cytometry. Scale bar = 200 μ m. (B) Flow cytometry histograms
1065 showing the percentage of cells in S/G2/M phases in *crestin:eGFP*-positive or
1066 *Tg(mitfa:eGFP)*-positive cell populations in BMPi-treated embryos compared to vehicle-
1067 treated embryos. (C) Fold change of *crestin:eGFP*-positive cells (top) and *mitfa:eGFP*-
1068 positive cells (bottom) in S/G2/M phases. n = 4 biological replicates of 80-100 stage-
1069 matched embryos pooled for each condition. Error bars represent mean +/- SEM, P-
1070 value calculated using ratio paired t-test, n.s., not significant.

Figure S3

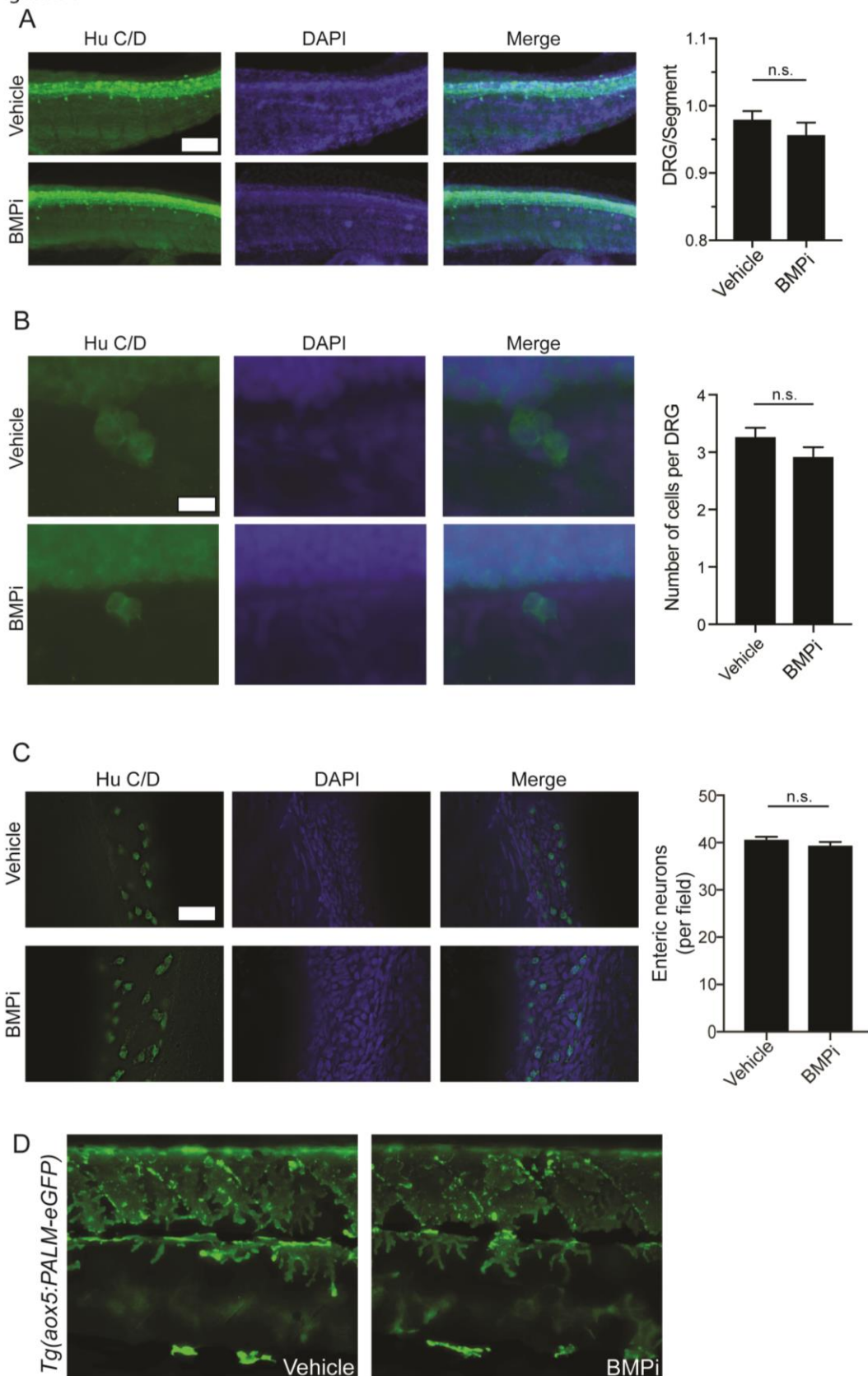


1071

1072 **Figure S3 (Related to Figure 3). Treatment with the BMP inhibitor DMH1 reduces**
1073 **phospho-SMAD1/5/8 staining in embryos**

1074 Top, vehicle-treated animals and, bottom, BMPi-treated animals. Photomicrographs for
1075 pSMAD-1/5/8-stained embryos were taken at the same exposure settings. Scale bar =
1076 50 μ m.

Figure S4



1078 **Figure S4 (Related to Figure 5). Some neural crest populations are unaffected by**

1079 **BMP inhibition**

1080 (A) Hu C/D staining for dorsal root ganglion structures showed no significant change in

1081 the number of dorsal root ganglia developing per segment, n = 5 per group. Scale bar =

1082 50 μ m. (B) Hu C/D staining for individual DRG's showed no significant change in the

1083 number of cells populating each individual DRG; n = 29 per group. Scale bar = 10 μ m.

1084 (C) Hu C/D staining for enteric neurons showed no significant change in number of

1085 enteric neurons per field in developing gastrointestinal tract; n = 4 per group. Scale bar

1086 = 50 μ m. (D) Qualitative evaluation of xanthophore development using *Tg(aox5:PALM-*

1087 *eGFP*) embryos treated with vehicle or BMPi showed no apparent change in density or

1088 localization of xanthophores between vehicle- and BMPi-treated embryos, supported by

1089 no change in *aox5* expression as shown in Figure 5A. Error bars represent mean +/-

1090 SEM. P-values were calculated using Student's t-test, n.s., not significant.

Figure S5

	Mel.	Irid.	
Veh.	71	30	101
BMPi	67	13	80
1091	138	43	181

$p < 0.05$

1092 **Figure S5 (Related to Figure 6). Quantification of iridophore and melanocyte**

1093 **numbers from lineage tracing**

1094 Number of iridophores and melanocytes identified by lineage tracing under each

1095 condition. P-value was calculated using Fisher's exact test, $P < 0.05$.